

4.0 Experimental Conditions and Burner Operation

4.1 Experimental Conditions

Ethylene was chosen as the nonpremixed flame fuel for this study because of its relatively strong sooting tendency [Glassman, 1988] and because it allowed direct comparison to other coflowing nonpremixed flame soot studies [Kent and Wagner, 1982 and Santoro *et. al.*, 1983]. The single mode flame conditions for this study were chosen to be similar to Kent and Wagner's [1982] "test 3" and "test 5" flames.

Hydrogen was the only premixed flame fuel considered in this study. Hydrogen offered simplicity in that its combustion would sufficiently heat the oxidizer while introducing water vapor as the only new chemical species in the oxidizer stream. Measurements by Zhang *et. al.* [1992] in a counterflow nonpremixed flame with vitiated oxidizer indicated that H₂O concentration in the oxidizer stream had a much greater effect on soot formation than CO₂. Considering hydrocarbon premixed flame fuels in the future would be a natural progression of this work. Hydrogen/oxygen/air premixed flame stoichiometries of 0.3 and 0.5 were chosen in continuity with the dual mode counterflow flame soot work of Aftel [1996].

Many researchers have documented the strong influence of flame temperature on soot formation [Glassman, 1988, ¹Kent and Wagner, 1984, ²Kent and Wagner, 1984 and ¹Wey et. al., 1984]. Identically matching the two-dimensional flame structures and resulting temperature fields between the single and dual mode cases was impossible. The hotter oxidizer for dual mode operation results in smaller temperature gradients near the reaction zone and therefore lower transverse diffusion velocities yielding much thicker flames than in single mode operation (Figure 4.1). It was decided to match *maximum* flame temperatures with height above the burner as closely as possible by adjusting the oxidizer index.

Table 4.1 Oxidizer Slot Flow Conditions

Case	Air Flow Standard cc/s	O ₂ Flow Standard cc/s	H ₂ Flow Standard cc/s	Oxygen Index*	Oxidizer Temp, K
Single Mode	35.6	1.4	0.0	0.24	400**
0.3 Dual Mode	52.9	1.6	7.6	0.15	1150
0.5 Dual Mode	53.9	6.5	17.8	0.13	1300

* post premixed flame for dual mode cases

** single mode oxidizer is slightly heated as it flows through burner

It was decided to study underventilated flames because most of the soot formation processes in practical flames occurs under locally fuel rich conditions. Overall stoichiometry of 2.0 was chosen because it allowed considerable flame stability margins for all cases given the “operating space” of the burner. Ethylene was used as the nonpremixed flame fuel for all cases at a flow rate of 11.9 standard cc/s (3.3 cm/s cold fuel slot velocity) requiring an oxygen flow (post premixed flame for dual mode cases) of

17.9 standard cc/s. Oxidizer flow conditions for the three flames considered are summarized in Table 4.1. Nitrogen coflows for single mode and dual mode cases were 75 cc/s and 19 cc/s respectively. Larger coflows aided single mode stability where smaller coflows were favored in dual mode operation.

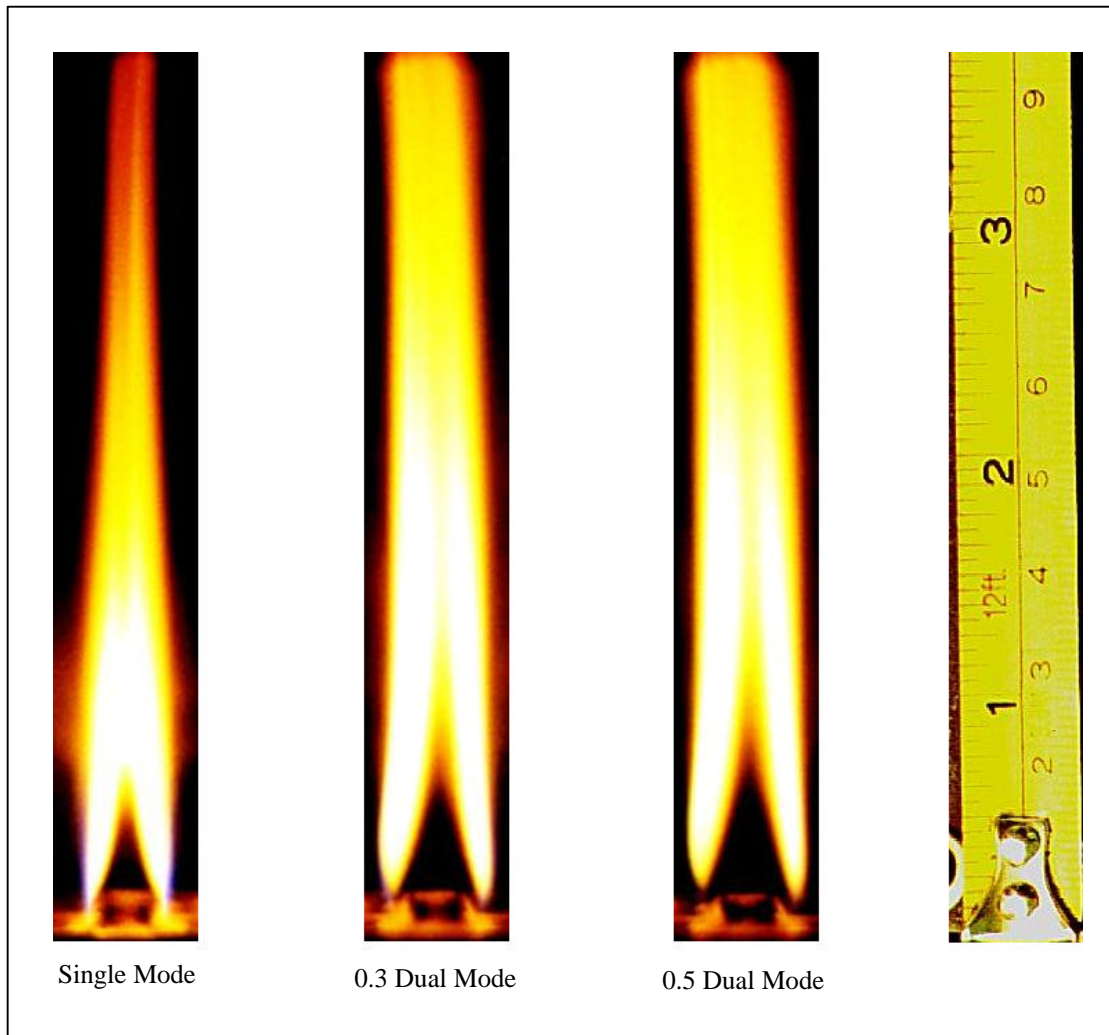


Figure 4.1 Wolfhard-Parker Flames

4.2 Burner Operating Procedures

4.2.1 Cooling Water

The burner became very hot during operation (especially in dual mode) and required cooling water through the hydrocarbon fuel slot and the outer water jacket. The right angle ball valve on the water manifold supplied cooling water to a coil in the hydrocarbon fuel slot. This valve should be "wide open" at the largest flow rate possible with the domestic water supply anytime before the burner is lit.

The throttling globe valve on the water manifold supplies cooling water to the coils comprising the outer water jacket. This valve should be open approximately 1/8 of a turn for 0.5 Dual Mode operation (hottest case) and just cracked for 0.3 Dual Mode and Single Mode operation. For the 0.5 Dual Mode flame more water is always better up to the point that the flexible hose connections to the burner begin to leak. Too much cooling water to the outer jacket in 0.3 Dual Mode and Single Mode can cause instability (not much more than a trickle is required to protect the burner).

Both cooling water flows should be visually verified at the drain before lighting the burner. Routinely monitor outer jacket cooling water return by touch. It should never be hotter than "warm."

4.2.2 Lighting the Burner

- Install the clean flame attachment/exit flow conditioning screen into the top of the burner at the correct height scribed onto the rear thermocouple access panel. Install the two side windows with their Fiberfrax seals. Too much torque on the window retaining pane screws can cause the windows to break when heated. Install the screws moderately hand tight and then back them out 1/8 turn. Never tighten them with a wrench.
- Set air rotameters to 73 on the glass float and nitrogen coflow rotameter to 8 on the glass float. Verify that the oxygen and *especially* hydrogen rotameters are **not** supplying flows to the burner.
- Light the portable propane torch. Supply the burner hydrocarbon fuel slot with Ethylene at a rotameter level of ~ 30 on the glass float. Light the burner with the propane torch. There may be a lag of ~10 seconds for the ethylene to reach the burner.
- Install the front window with its Fiberfrax seal.

4.2.3 Stabilizing the flame

The hydrocarbon diffusion flame must be coaxed into attaching to the exit screen before operating steadily without flicker. This stabilization is most easily and quickly accomplished for the 0.5 Dual Mode flame.

- Continuing from Section 4.2.2. Set oxygen rotameters to 84 on the glass float.

- Adding hydrogen to the oxidizer slots too rapidly can cause the windows to crack. The final target hydrogen flow rate for 0.5 Dual Mode operation is 78 on the glass float but initially light the hydrogen premixed flames at a rotameter setting of ~60 on the glass float. After several minutes with the hydrogen rotameters at 60 on the glass float move them up to the final flow of 78 on the glass float. Water condensation on the glass is typical.
- Advance the ethylene rotameter setting from ~30 on the glass float, where it was lit, to ~55 on the glass float. This is less than the final target ethylene rotometer setting of 90 on the glass float but a lower flow rate aids flame stabilization and keeps the windows cleaner during flame stabilization.

The diffusion flame may be coaxed into stable operation by turning the nitrogen coflow on and off ("on" being 8 on the rotameter glass float) with a period of about 30 sec to 1 min. This procedure takes about 10 min. Turning the coflow on will appear to disturb the flame with stability improving every time the coflow is shut off.

When the burner operates steadily with coflow on raise the ethylene rotometer setting to its final value of 90 on the glass float. This is the 0.5 Dual Mode case. Once this case has been stabilized the burner flow rates may be changed to either of the other two test cases without losing stability for the most part.

4.2.4 Burner Operation Notes

When reducing the stoichiometry of the oxidizer slot premixed flames (going from 0.5 Dual Mode to either other case) adjust the hydrogen flow rate first followed by oxygen and then air. When increasing the stoichiometry of the oxidizer slot premixed

flames do just the opposite by adjusting the air followed by oxygen and then hydrogen. This order of operation will ensure that the burner is not operated with premixed flame stoichiometry greater than 0.5.

The diffusion flame can be unstable in two different but equally undesirable modes. The flame can flicker in the vertical direction and sway in the horizontal direction. The higher the Nitrogen coflow the more margin you have against side to side swaying of the flame. The lower the Nitrogen coflow the more margin you have against vertical flickering. The Nitrogen coflow rates listed previously are recommendations known to promote overall flame stability.

4.2.5 Burner Shutdown

- Turn off the gas flows to the burner in the following order: Hydrogen, Ethylene, Oxygen and Nitrogen.
- Leave air flowing through the oxidizer slots at a rotometer setting of about 30 on the glass float for 15 - 20 minutes to help cool the porous sinters. Also allow the cooling water to flow for about the same period of time after the flame is extinguished.
- Leave the windows on until they are cool to the touch. Rapid cooling can cause them to crack

5.0 Results and Discussion

5.1 Temperature

The corrected gas temperature fields, calculated from thermocouple thermometry measurements, are shown in Figure 5.1 with the correction magnitudes, $(T_{\text{gas}} - T_{\text{thermocouple}})$ plotted in Figure 5.2. The highest radiation corrections, ~160 K, occur near the base of the flames where low velocities result in small convection coefficients around the junction and near the flame front where the thermocouple radiates most strongly due to high surface temperature.

The gas temperature fields offer insight into the differences in flame structure among the three flames considered in this study. Notice the transverse broadening of the flames for increasing degrees of dual mode operation consistent with the broadening of the luminous sooting regions shown previously in Figure 4.1. Figure 5.1 shows that the single mode flame front (peak temperature) lies 5 mm from centerline whereas both dual mode flame fronts lie near 7 mm. Dual mode operation elongates the flame front evident by the axial stretching of the peak temperature “cores.” The need for flow conditioning and a

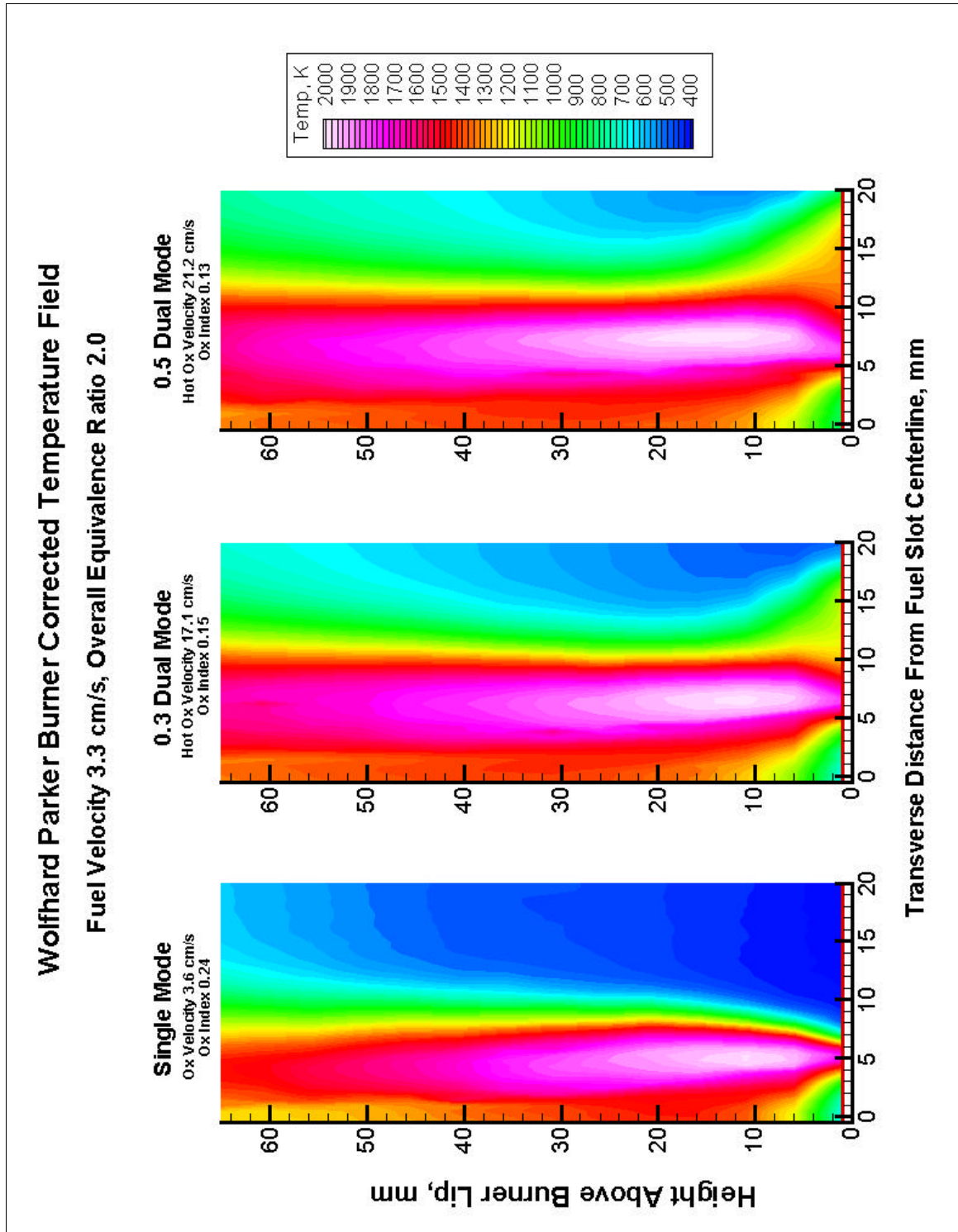


Figure 5.1 Corrected Temperature Fields

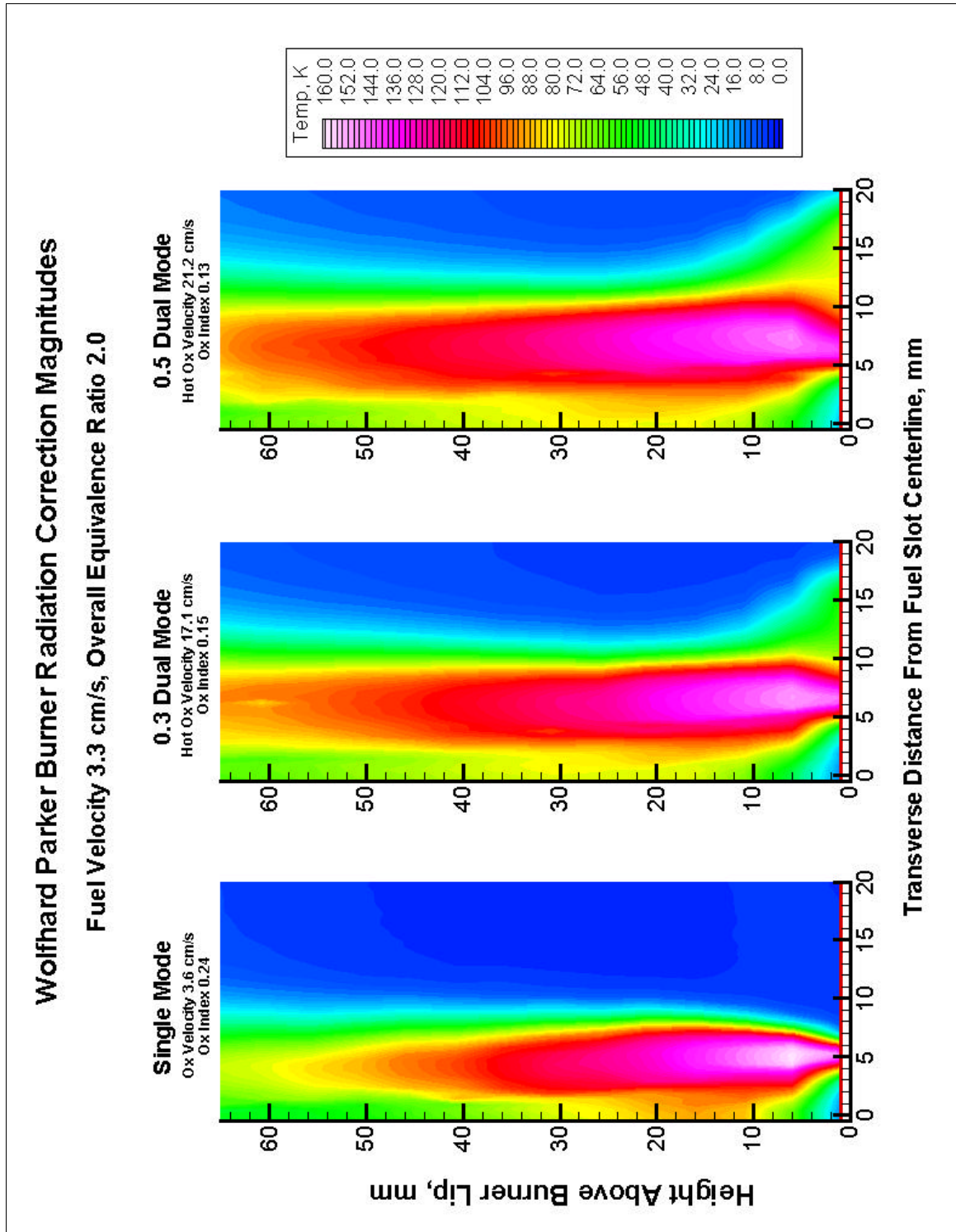


Figure 5.2 Temperature Correction Magnitudes

flame stabilizing screen above the burner prevented determination of true luminous flame heights.

As mentioned previously in section 4.1 one of the major factors governing the selection of experimental conditions was matching peak temperatures among the cases. Figure 5.3 shows maximum and centerline temperatures for the three flames considered as a function of height above the burner. All three flames have peak temperatures of approximately 1990 K at surprisingly identical heights of 10 mm. This peak temperature agrees with peak corrected temperatures near 2000 K measured in a similar ethylene flame by Kent *et al.* [1981].

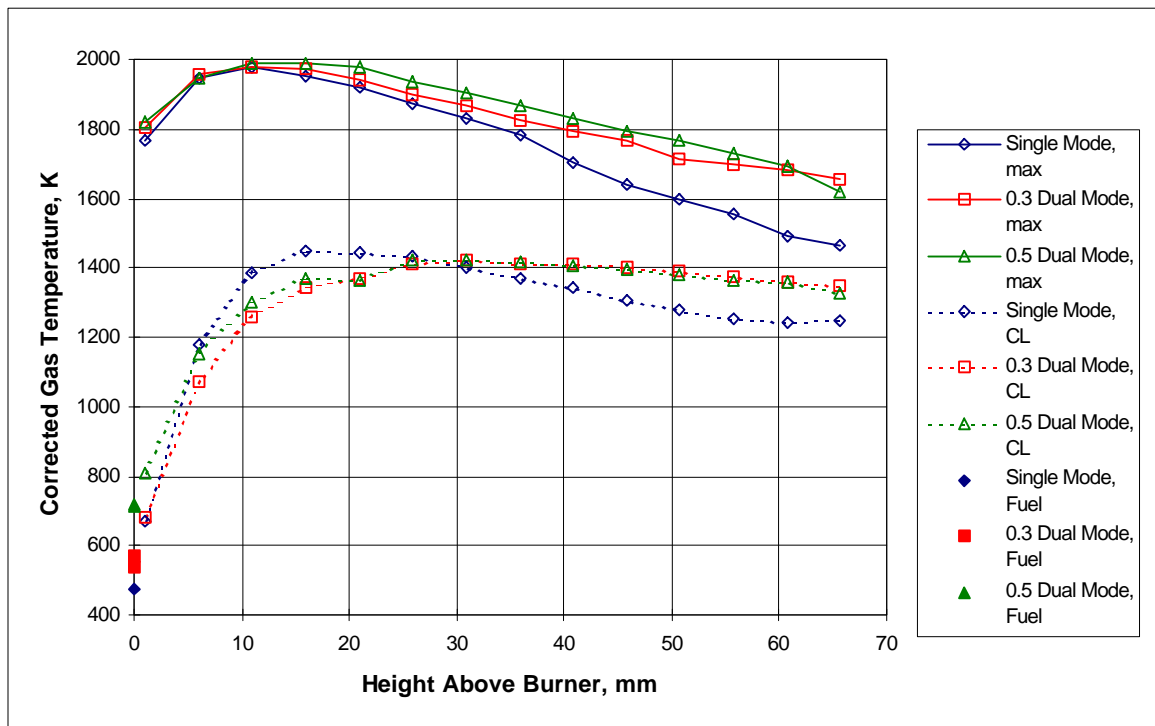


Figure 5.3 Maximum and Centerline Temperatures

The radiation corrections applied in Kent *et al.* [1981] assumed a junction radiant emissivity of 0.3 and a Nusselt number of 2.0 (spherical geometry); both decisions ungrounded and without discussion. A radiant emissivity of 0.3 is large compared to measurements of just over 0.2 reported by Bradley and Entwistle [1966] tending to overestimate the radiation correction by ~30%. The assumption of junction spherical convective behavior, $Nu = 2.0$, could underestimate the radiation correction by as much as 100% if the thermocouple actually behaved more like an infinite cylinder. Although the radiation corrections may have been well underestimated, as much as 70%, it is reasonable that the maximum temperatures in Kent *et al.* [1981] agree with the present study because their flames were well overventilated where the flames in this study were underventilated perhaps producing lower flame temperatures.

The higher sensible energy in the dual mode oxidizers sustain the peak temperatures at higher values after the absolute peak near 10 mm. Recall that the oxidizer flow for the single mode case had to be oxygen enriched and that the heated oxidizers for the dual mode cases remained diluted with combustion products to match the overall peak nonpremixed flame temperatures. Figure 5.4 showing temperature profiles at a height of 1mm, just over the burner lip, illustrates the differences in the thermal boundary conditions at the burner lip for the three flames. Temperature profiles at heights of 20 mm, 40 mm and 60 mm are shown in Figure 5.5. Uncertainties in the calculated gas temperatures (Appendix D) were all less than 4%. A scatter plot of the error bar magnitudes for all three flames are plotted versus corrected temperature in Figure 5.6.

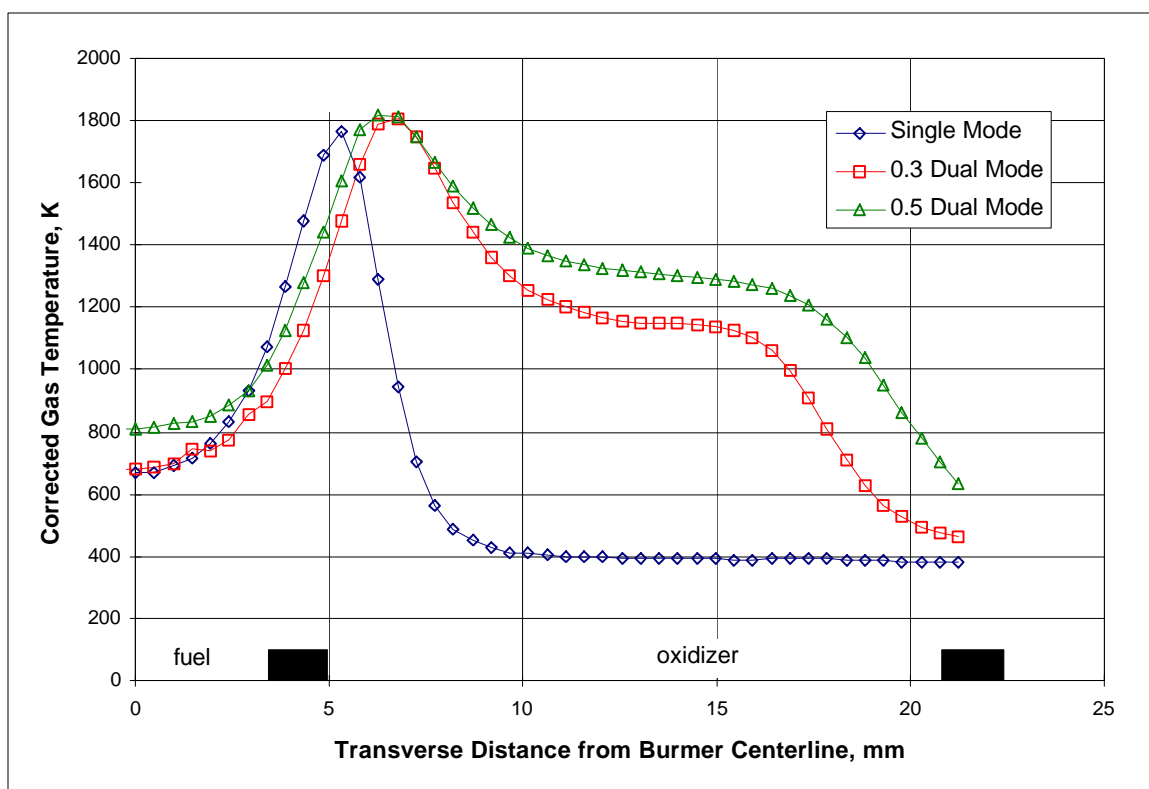


Figure 5.4 Transverse Temperature Profiles, Height 1mm

Notice also from Figure 5.4 that although the fuel slot was water cooled there was considerable heating of the fuel before leaving the burner. Ceramic honeycomb flow conditioning for the fuel slot rested flush with the upper lip of the fuel slot preventing direct measurement of fuel temperature before leaving the burner. The “height zero” fuel temperatures, shown as solid symbols on Figure 5.3, were estimated using a transient technique. At the end of several tests the thermocouple was positioned 1mm above and on centerline with the fuel slot and a temperature-time trace was collected as the oxidizer flows were turned off extinguishing the flame but allowing the fuel to continue to flow. Using sharp changes in slope of the temperature-time traces, shown in Figure 5.7, to indicate when the flame was extinguished an average of the following 5 seconds were

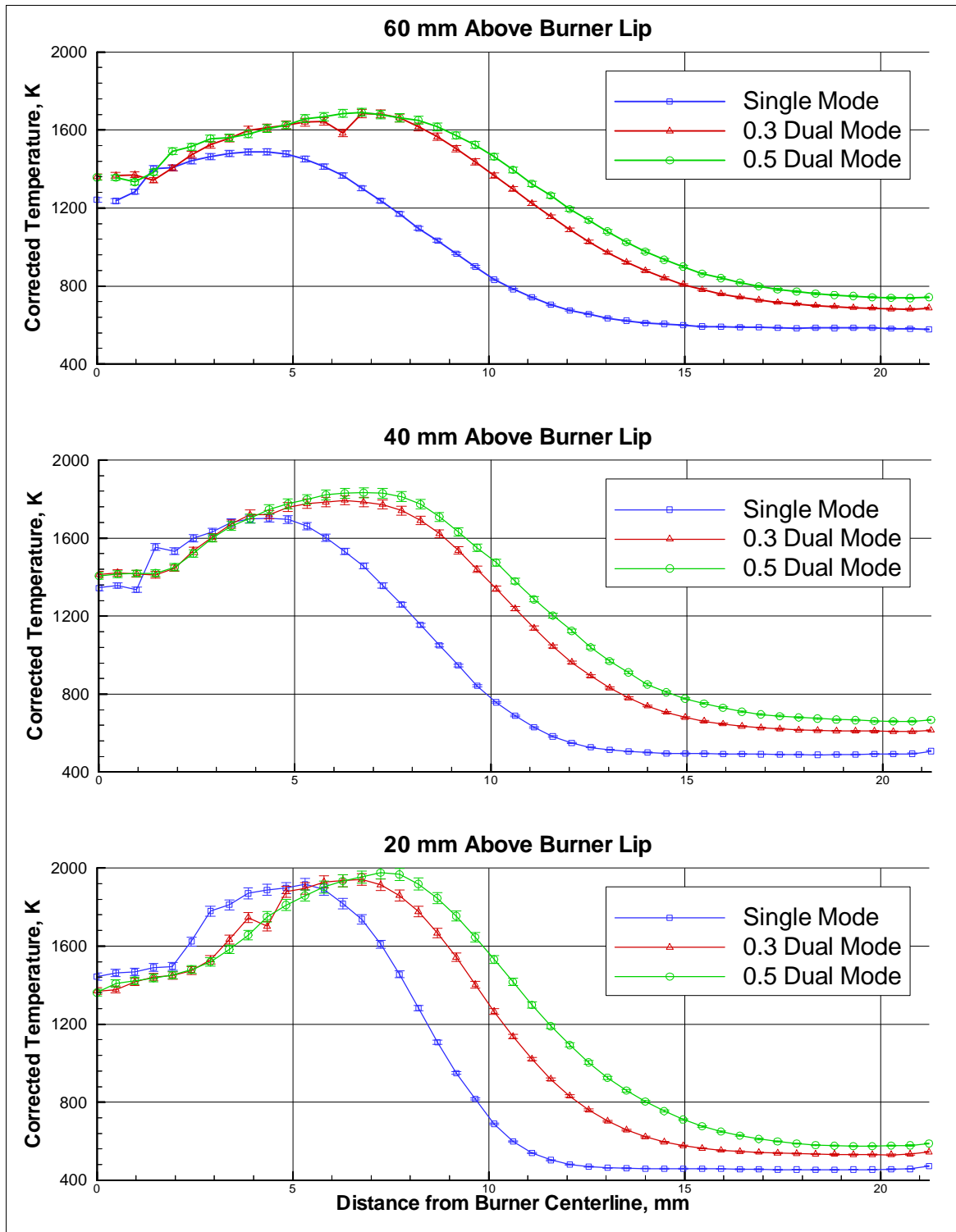


Figure 5.5 Corrected Gas Temperature Profiles at Various Heights

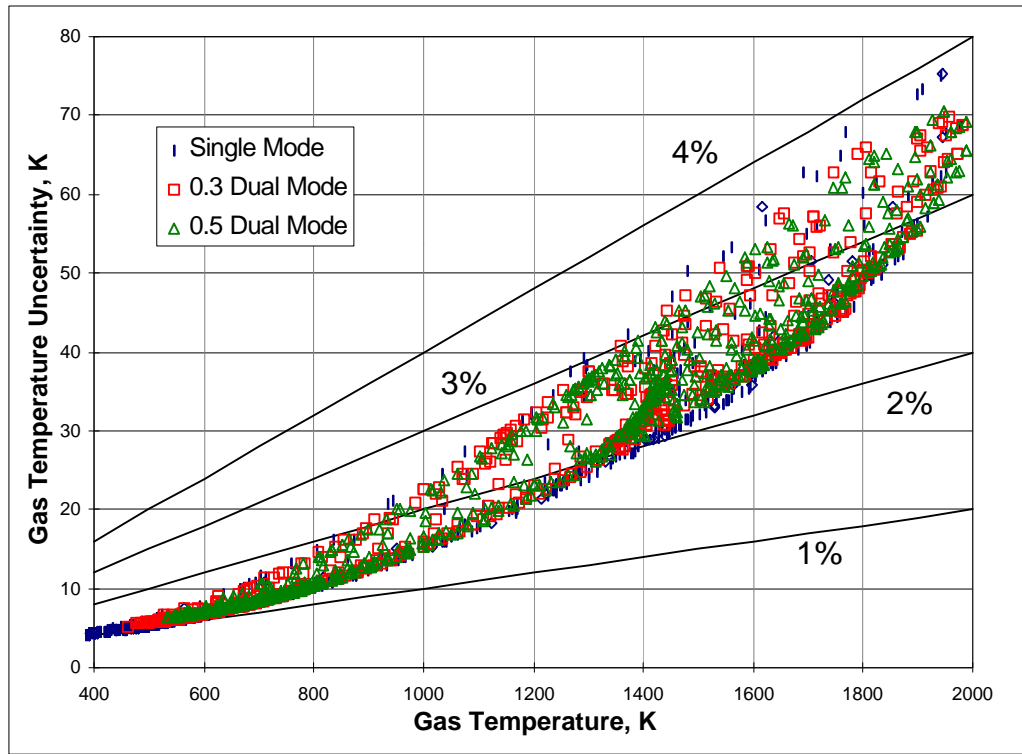


Figure 5.6 Gas Temperature Uncertainty Versus Gas Temperature

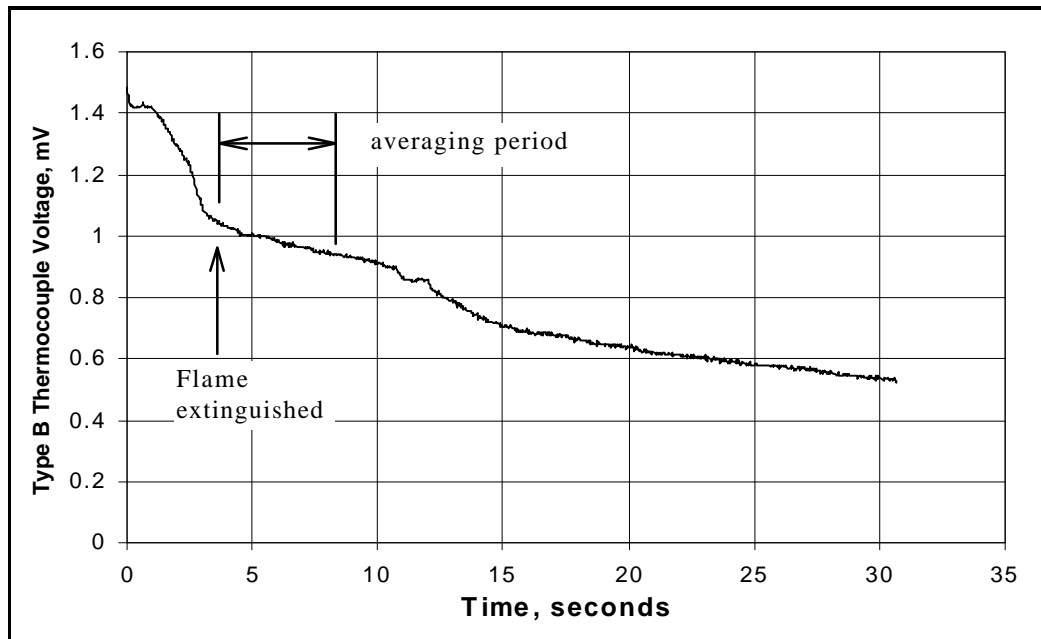


Figure 5.7 Thermocouple Output Voltage as Flame Extinguishes

taken as an approximation of the fuel temperature at zero height just before leaving the burner. Notice that the zero height fuel temperatures dropped with decreasing premixed flame stoichiometry likely the result of lower burner surface temperatures.

Figure 5.8 illustrates the differences in the transverse temperature slopes for the three flames. Notice that the single mode flame has much steeper temperature gradients on both the fuel and oxidizer sides of the flame with exception for spikes in the dual mode cases near 5mm. The higher temperature gradients in the single mode flame certainly cause faster heat diffusion rates. The single mode centerline temperatures rising above the dual mode centerline temperatures for heights < 30 mm, shown in Figure 5.3, also demonstrates the more rapid heat diffusion in the single mode flame.

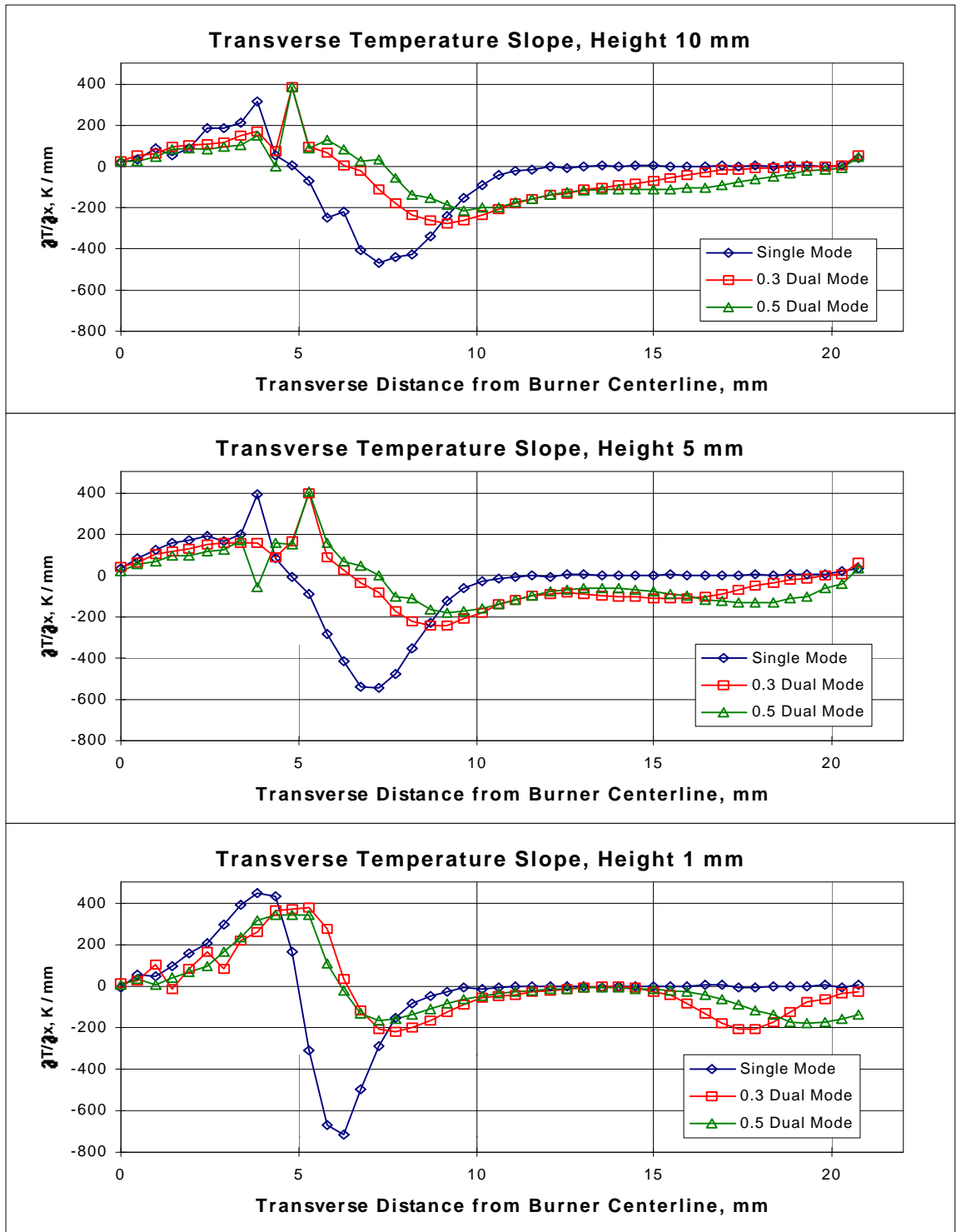


Figure 5.8 Transverse Temperature Gradients at Various Heights

5.2 Thermocouple Particle Densitometry Soot Volume Fraction

Soot volume fraction measurements by Thermocouple Particle Densitometry (TPD) [McEnally *et. al.*, 1997] as discussed in Appendix A.4 were made simultaneously with temperature. Results from TPD analysis of the temperature-time traces, shown in Figure 5.9, indicate that soot volume fractions decrease and the soot laden region width increases for increasing degrees of dual mode operation. Peak soot volume fraction in the single mode case is approximately 8 ppm where the peaks in the dual mode cases are down just over 4 ppm.

Performing TPD analysis simultaneously (in space and time) with thermocouple thermometry facilitates comparison between the spatial features of each measurement. Figure 5.8 shows that the onset of appreciable soot volume fractions, $\phi > 1\text{ppm}$, typically rides the 1600 K isotherm for all three cases. This observation can be interpreted as evidence that there is an activation energy associated with soot particle nucleation.

The same data from Figure 5.9 is plotted again in Figure 5.10 with a logarithmic color map to emphasize the lower soot concentrations. Notice the void in the centerline soot volume fractions of the dual mode cases near a height of 20 mm. This was a curious and repeatable feature of all dual mode TPD measurements.

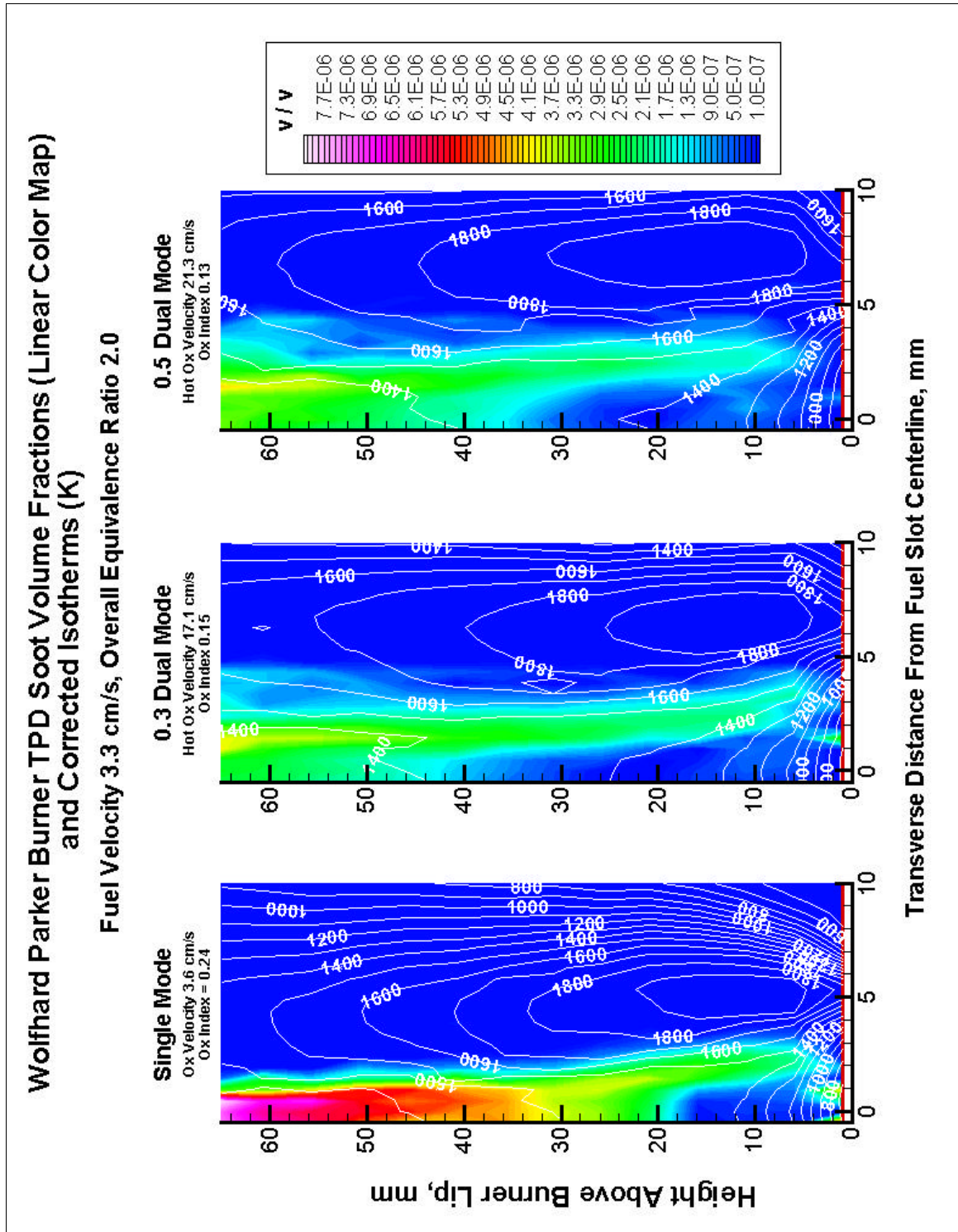


Figure 5.9 TPD Soot Volume Fractions (linear color map) with Isotherms

**Wolfhard Parker Burner TPD Soot Volume Fractions (Log Color Map)
and Corrected Isotherms (K)**

Fuel Velocity 3.3 cm/s, Overall Equivalence Ratio 2.0

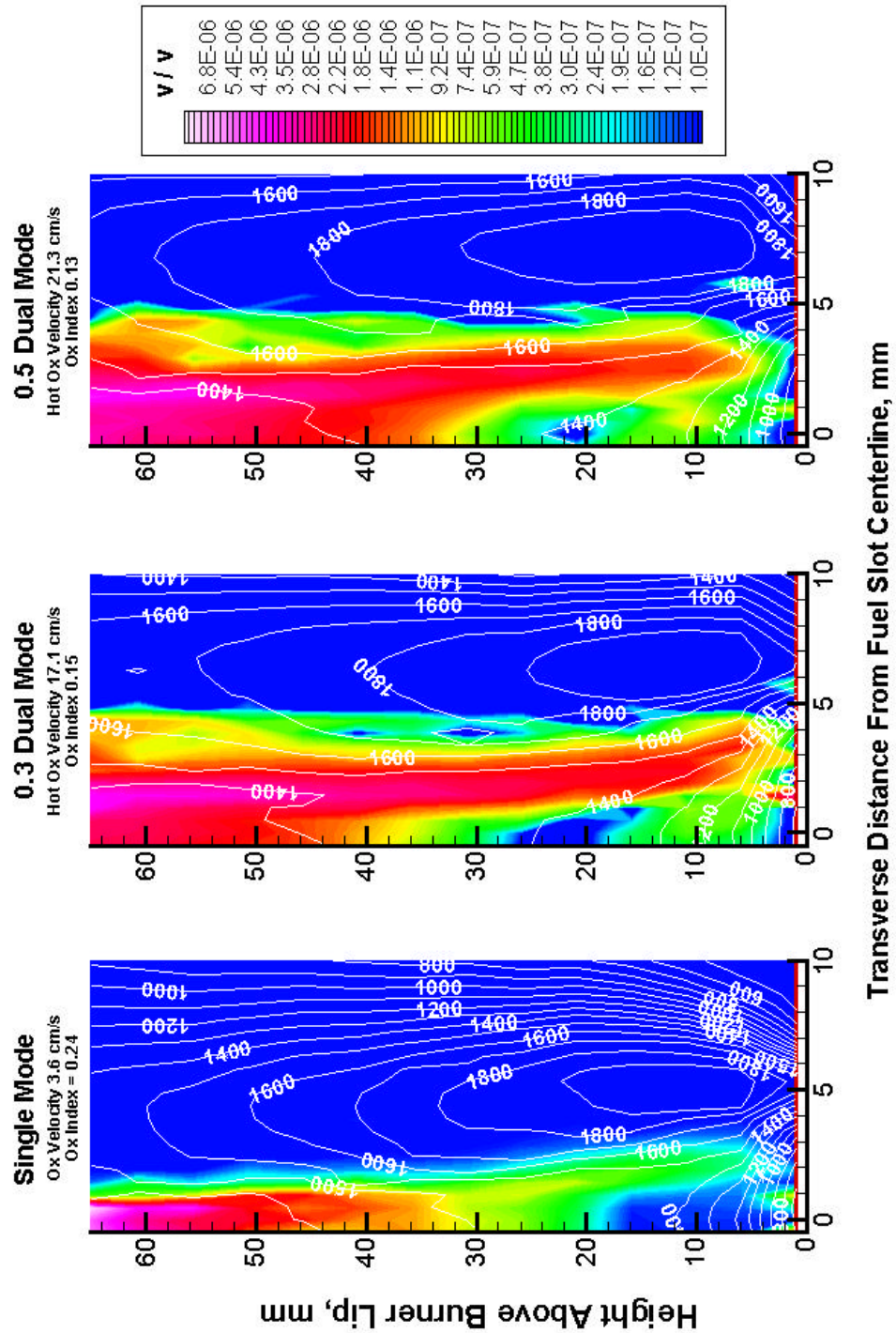


Figure 5.10 TPD Soot Volume Fractions (log color map) with Isotherms

5.3 Laser Light Scattering and Extinction

5.3.1 Laser Light Extinction (LLE)

Flood plots of soot volume fraction derived from laser light extinction measurements are shown in Figure 5.11 with a linear color map and in Figure 5.12 with a logarithmic color map emphasizing the lower soot volume fractions. Identical to the TPD soot volume fractions the extinction measurements show a trend of lower soot volume fractions and wider soot laden regions for increasing degrees of dual mode operation.

Figures 5.13 shows plots of transverse soot volume fraction profiles for heights of 20mm, 40mm and 60mm above the burner. Notice that the 0.3 Dual Mode and Single Mode soot laden regions lies a similar distance from centerline with the 0.5 dual mode soot laden region sitting further away from centerline. The peaks in soot volume fraction are very steep for the single mode case with softer peaks for the dual mode cases. A scatter plot of laser extinction soot volume fraction measurement uncertainties versus soot volume fraction, Figure 5.14, reveals a linear relationship with a slope of ~12%. Considerable scatter in the data existed for beam extinction less than 5 % ($I / I_0 > 0.95$) suspected to be the result of imperfections in the extinction path windows and particles suspended in coflow recirculation regions. Measurements of extinction values less than 5%, corresponding to soot volume fractions less than 2×10^{-7} , should be disregarded.

The TPD (Figures 5.9 and 5.10) and laser extinction (Figures 5.11 and 5.12) soot volume fraction distributions are nearly indistinguishable by comparison of the dual mode cases in both shape and magnitude. Agreement for the single mode case is not as close but the two methods still compliment one another. TPD appears to have underestimated

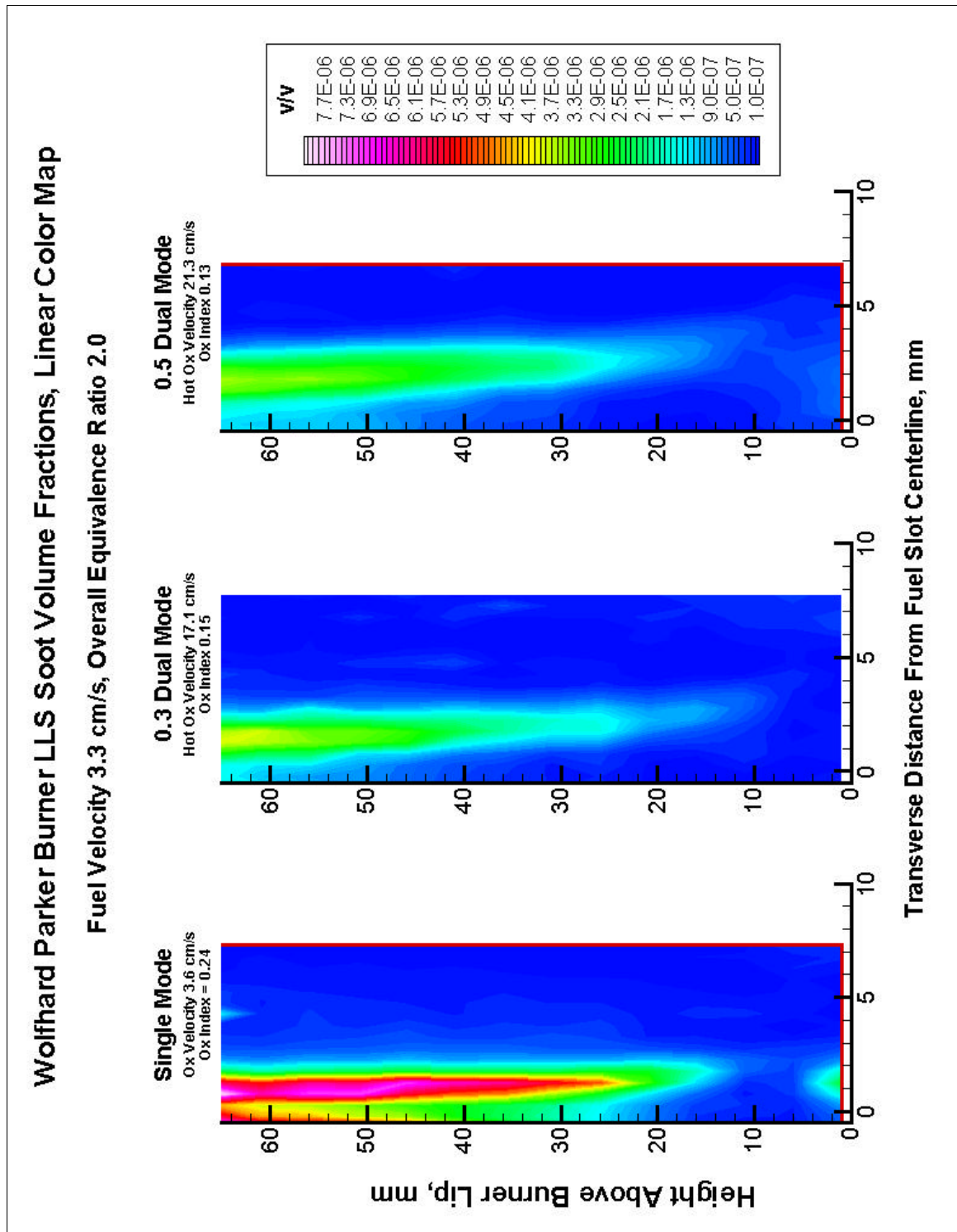


Figure 5.11 Laser Extinction Soot Volume Fraction (Linear Color Map)

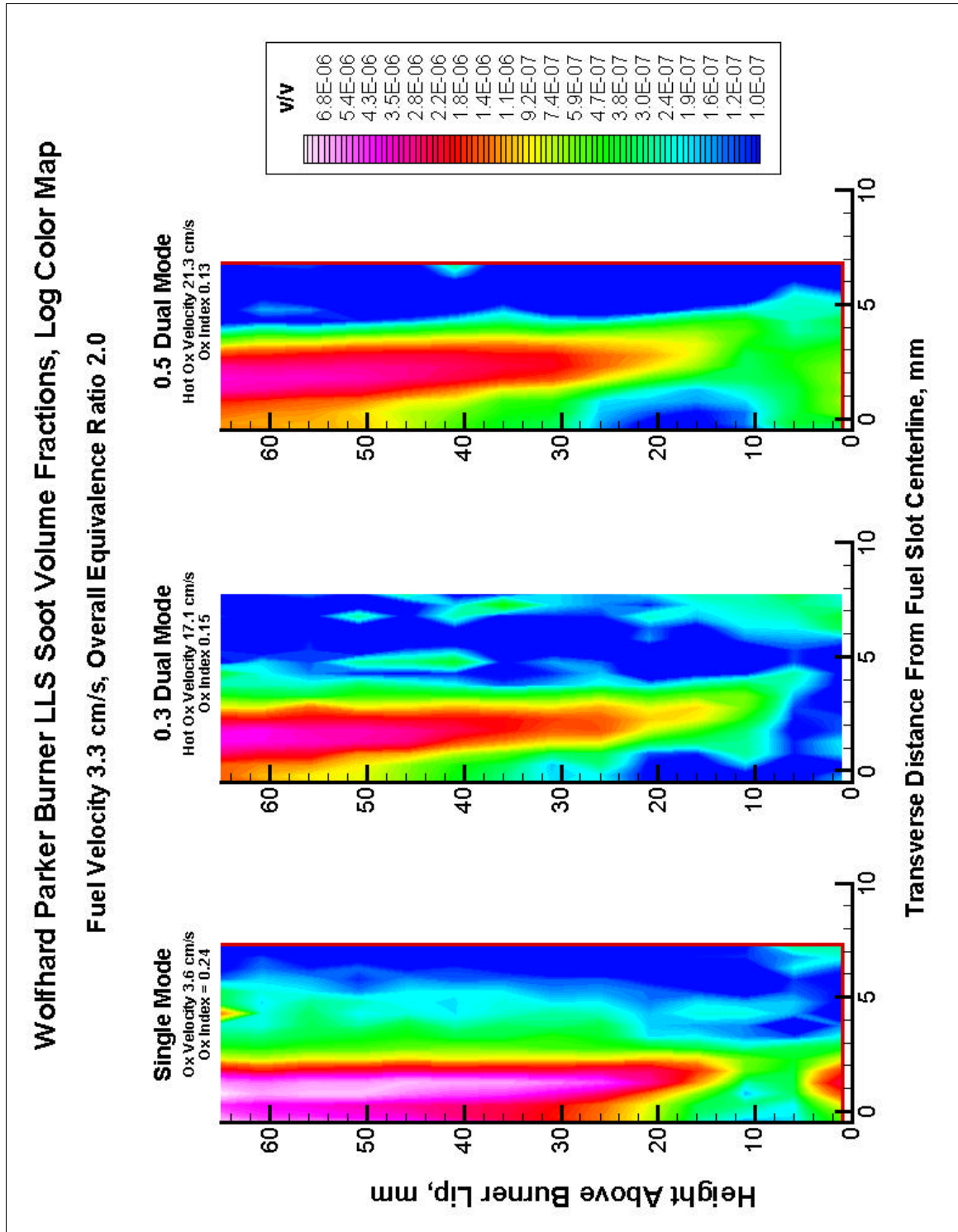


Figure 5.12 Laser Extinction Soot Volume Fraction (Log Color Map)

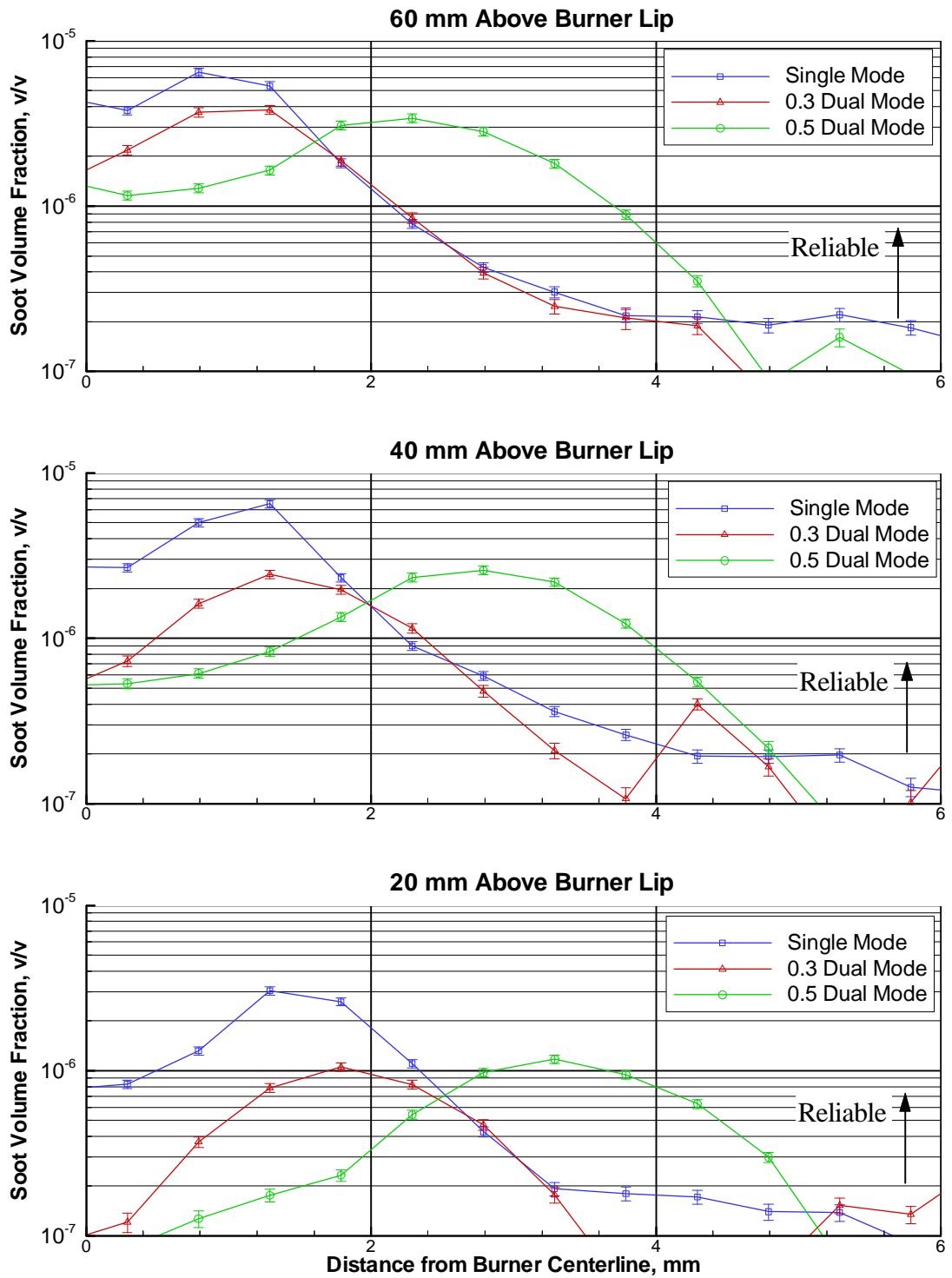


Figure 5.13 LLE Soot Volume Fraction Profiles at Various Heights

the peak soot volume fractions low in the flame, below 30 mm, but indicates centerline soot earlier than the laser extinction method.

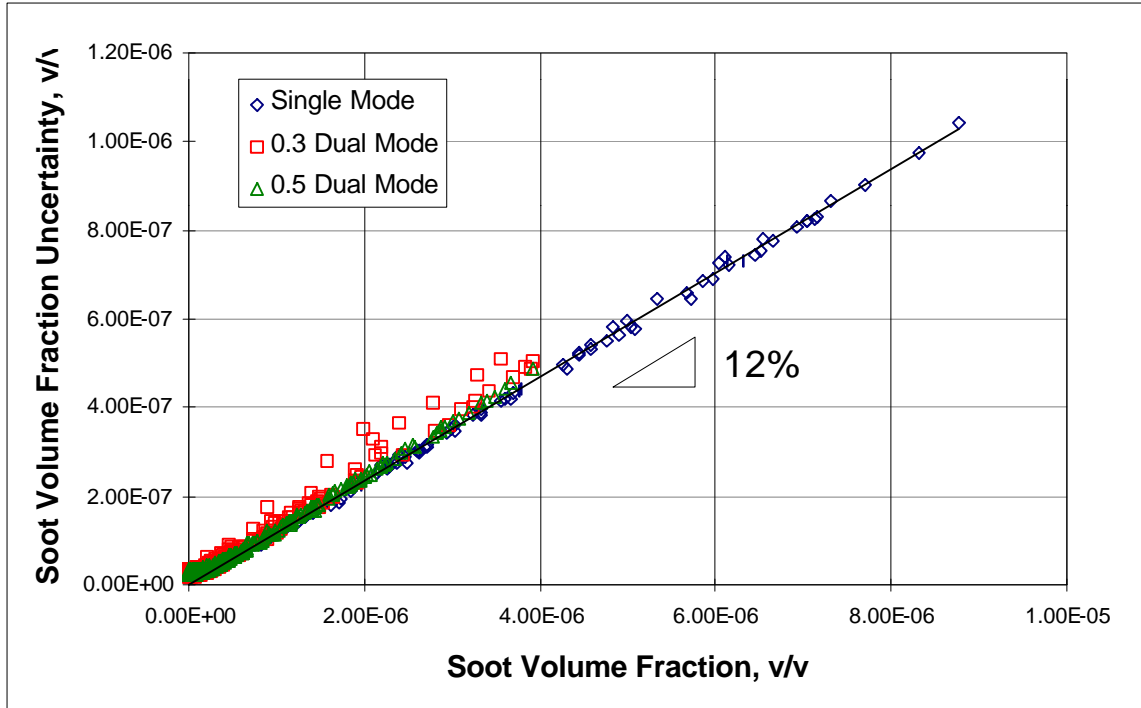


Figure 5.14 Soot Volume Fraction Uncertainty vs. Soot Volume Fraction

Earlier detection of particles on centerline by TPD may not be in error but perhaps a result of the method's claimed sensitivity to heavy but optically translucent aromatics [McEnally *et. al.*, 1997]. Measurements of Polycyclic Aromatic Hydrocarbon (PAH) fluorescence in the flame would be necessary to validate or refute this claim.

The 0.5 dual mode laser light extinction soot volume fraction distribution (but not so much the 0.3 dual mode case) with a logarithmic color map, Figure 5.12, showed the same soot free pocket on centerline at a height of 20 mm as observed in TPD measurements, Figure 5.10. The soot free pocket surrounded by small but measurable soot volume fractions indicates strong soot oxidation in that region. Whether the

oxidation is driven by molecular oxygen or hydroxyl radicals formed from water vapor is unclear without species measurements.

Figure 5.15 shows peak values of soot volume fraction as a function of height for both the TPD and LLE measurement techniques. Soot volume fraction peak values for both the dual mode cases increase linearly with height to nearly identical values, $\sim 4 \times 10^{-6}$. The single mode peak soot volume fractions rise very steeply before leveling off to a shallower slope (similar to that of the dual mode cases) at a height of 25 mm. The ceramic honeycomb flow conditioning and fuel slot lip appeared to locally promote pyrolysis of the fuel observed as slight carbon build up on the honeycomb and the high peak soot volume fraction values just above the burner lip (Figure 5.15).

The peak values of soot volume fraction measured by TPD and LLE show good agreement with one another in Figure 5.15. For the dual mode cases TPD yields slightly higher values of soot volume fraction. TPD did not show the change in slope of peak soot volume fractions in the single mode case as LLE measurements did. Still, TPD yields remarkable similarity to LLE considering the fundamental differences in theory behind each technique (heat and mass transport versus optical absorption).

Data for a flame similar to this study's Single Mode flame reported by Kent and Wagner [1982] are plotted in Figure 5.15 with '+' data markers demonstrating encouraging agreement between the two sets of measurements. It is reasonable that the maximum soot volume fractions for the *overventillated* Kent and Wagner [1982] flame reached higher values than those in the present study's *underventillated* Single Mode flame. Also since the Kent and Wagner [1982] flame is overventillated its maximum soot

volume fraction profile exhibits a local maximum resulting from soot particle oxidation high in the flame. The maximum soot volume fraction profile for the underventilated Single Mode flame in this study did not exhibit the same local maximum likely because all of the oxygen was either consumed or greatly diluted by the higher regions of the flame.

Differences between the Lorentz-Mie analysis of scattering and extinction data performed by Kent and Wagner[1982] and the Rayleigh analysis used in the present study are expected to result in only negligible differences in the soot volume fraction calculation. Although many of the particles in the current study were too large to strictly satisfy Rayleigh assumptions (Section 5.3.2) the extinction of the laser beam by scattering still should have been much smaller than extinction by absorption.

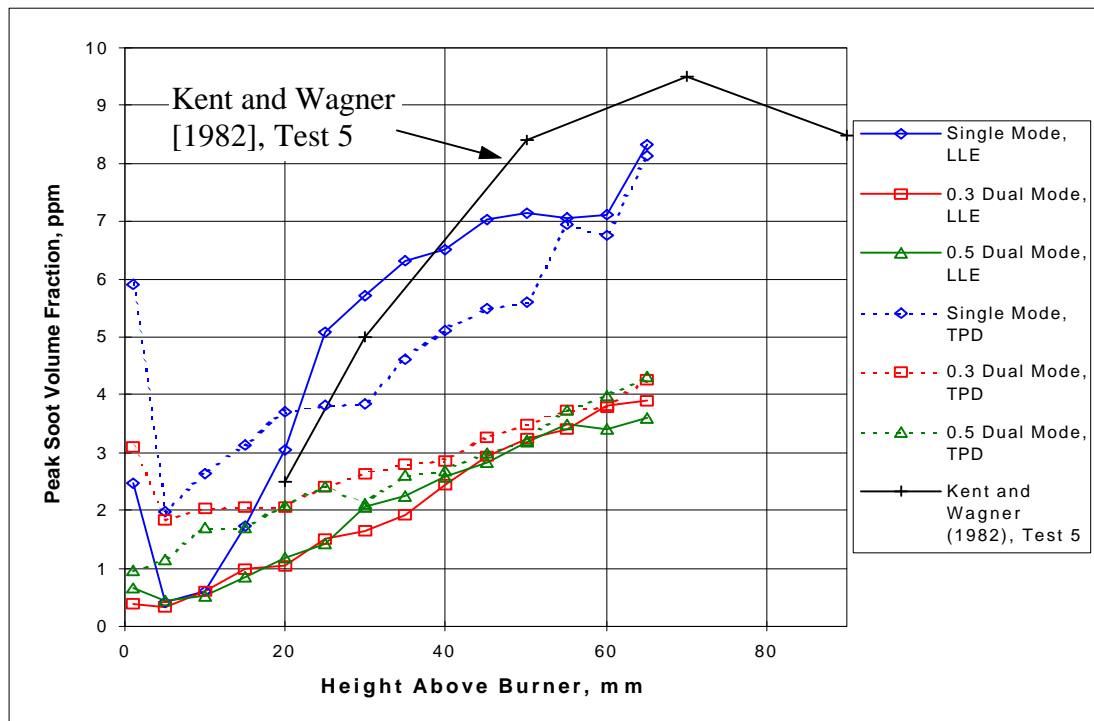


Figure 5.15 Soot Volume Fraction Peak Values vs. Height

5.3.2 Laser Light Scattering (LLS) Soot Particle Diameters

The flood plots of soot particle diameters in Figure 5.16, transverse profiles at various heights in Figure 5.17 and soot particle diameter peak values in Figure 5.18 indicate similar soot particle diameters for the single mode and 0.3 dual mode cases. The largest soot particle diameters were measured in higher regions of the 0.5 dual mode case.

Comparing the Single Mode flame maximum soot particle diameters to those reported by Kent and Wagner [1982] for their Test 5 flame in Figure 5.18 reveals good agreement in magnitude with a spatial shift toward larger heights for the Kent and Wagner [1982] data. Kent and Wagner [1982] report an overall maximum diameter of 145 nm calculated by full Lorentz-Mie analysis which is greater than the 132 nm overall maximum diameter reported for the Single Mode flame in the present study calculated using the Rayleigh limit assumption. Although Kent and Wagner [1982] report larger diameters than those in the present study one would expect the difference to be even greater considering the differences in optical scattering and extinction analysis.

Recall from Section 3.5.2 that the Rayleigh scattering assumption (scattering particles being much smaller than the wavelength of incident light, Equation 3.1), used in the analysis to determine these reported soot particles diameters, quickly loses its accuracy for particles greater than 100 nm. No uncertainty analysis was performed on soot particle diameter measurements since the Rayleigh assumption error surely dominated the overall uncertainty. However it is worth noting that the standard deviations of the scattering signals were typically $< 10\%$ with good repeatability from test to test.

While qualitative comparison of particle diameters outside the Rayleigh limit is plausible, caution must be used in interpreting relative magnitudes since the error rises non-linearly. In addition it is important to recall that the concept of soot particle “diameter” is a spherical idealization of non-spherical chains and clusters of soot particles as shown by Tunneling Electron Microscopy imaging of soot particles [Vander Wal, 1997]. It is perhaps more appropriate to refer to the soot particle size measurements as effective spherule diameters [Wey et. al., 1984b].

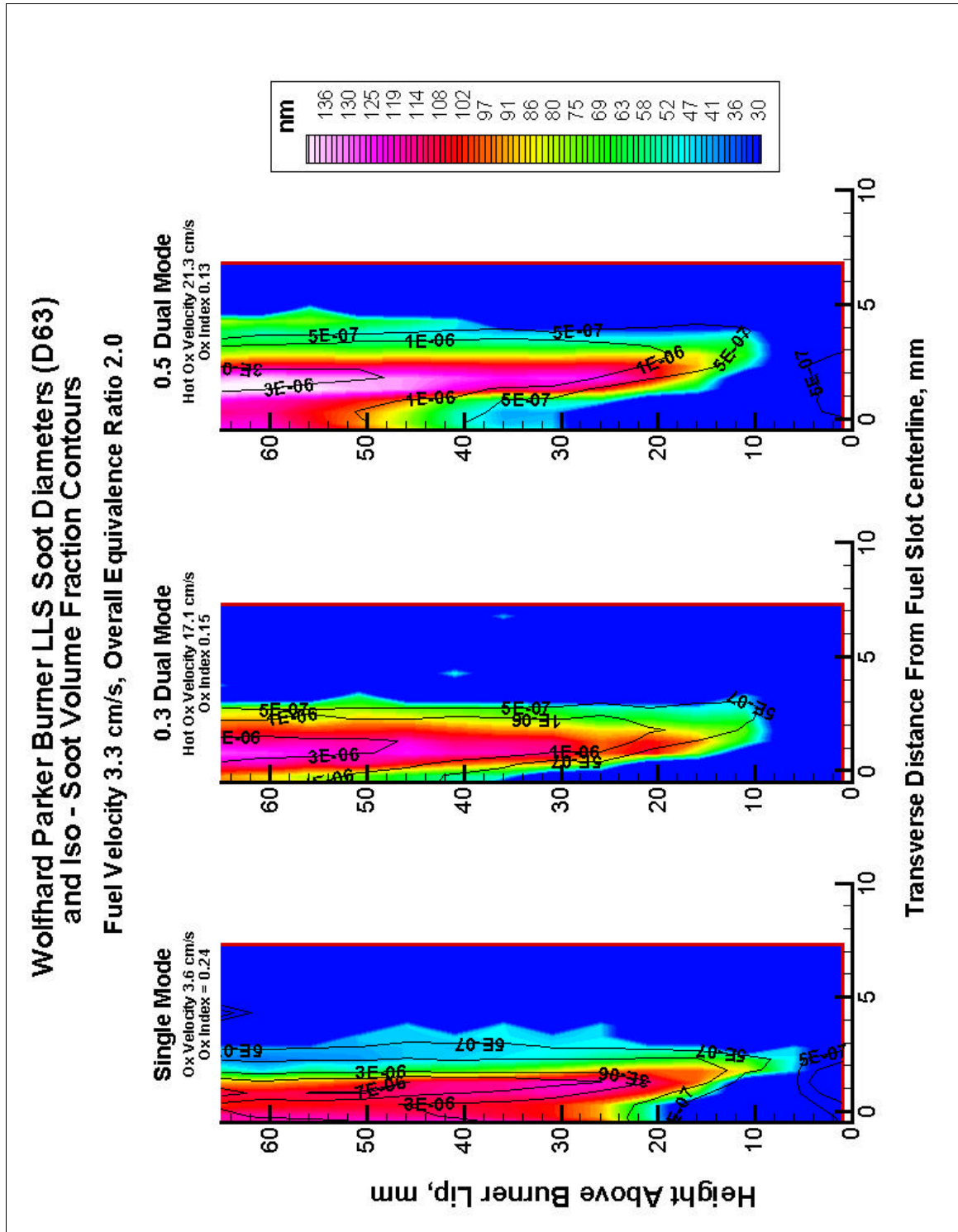


Figure 5.16 Light Scattering Measurements of Soot Particle Diameter (D_{63})

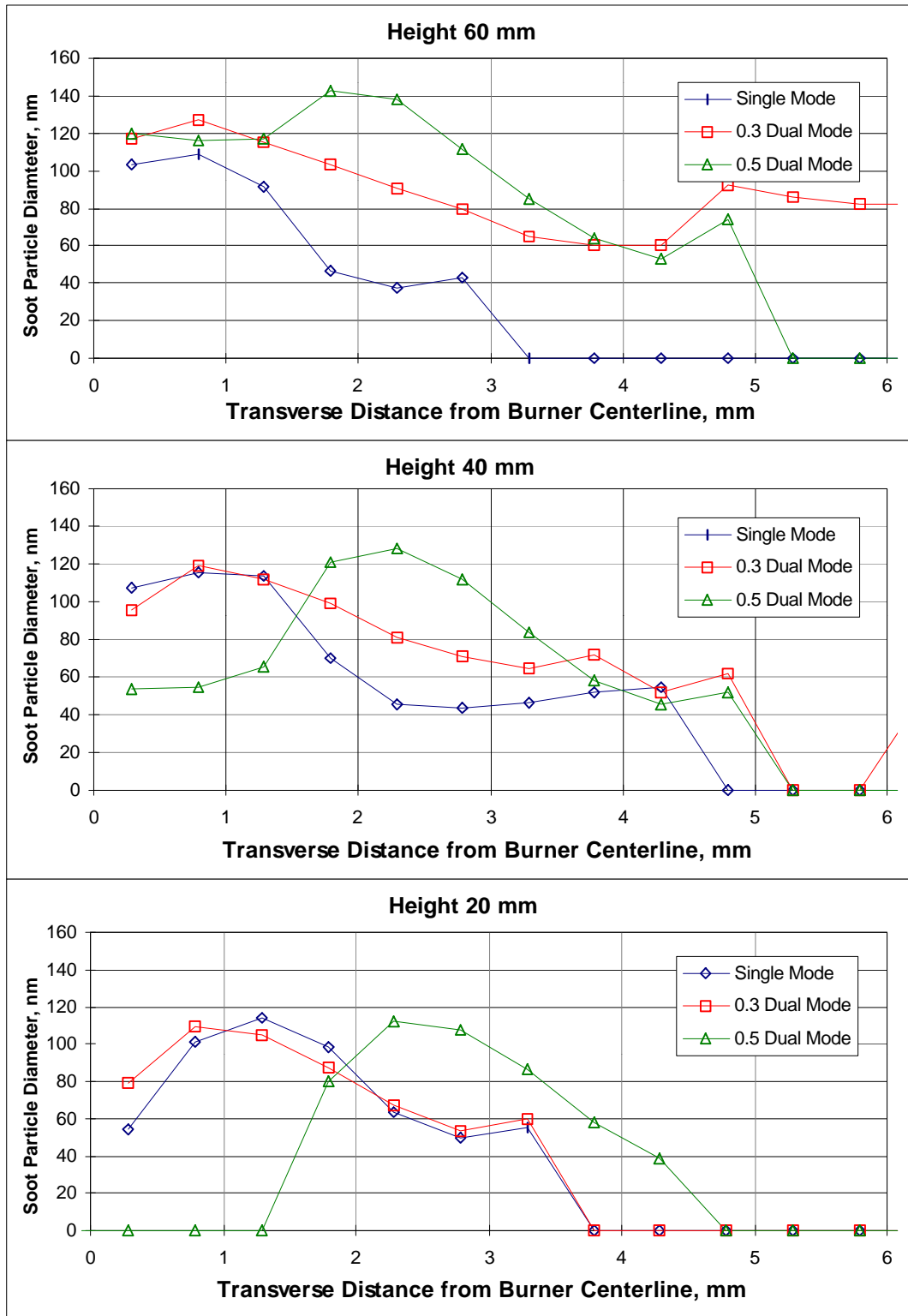


Figure 5.17 LLS Soot Particle Diameters (D_{63}) at Various Heights

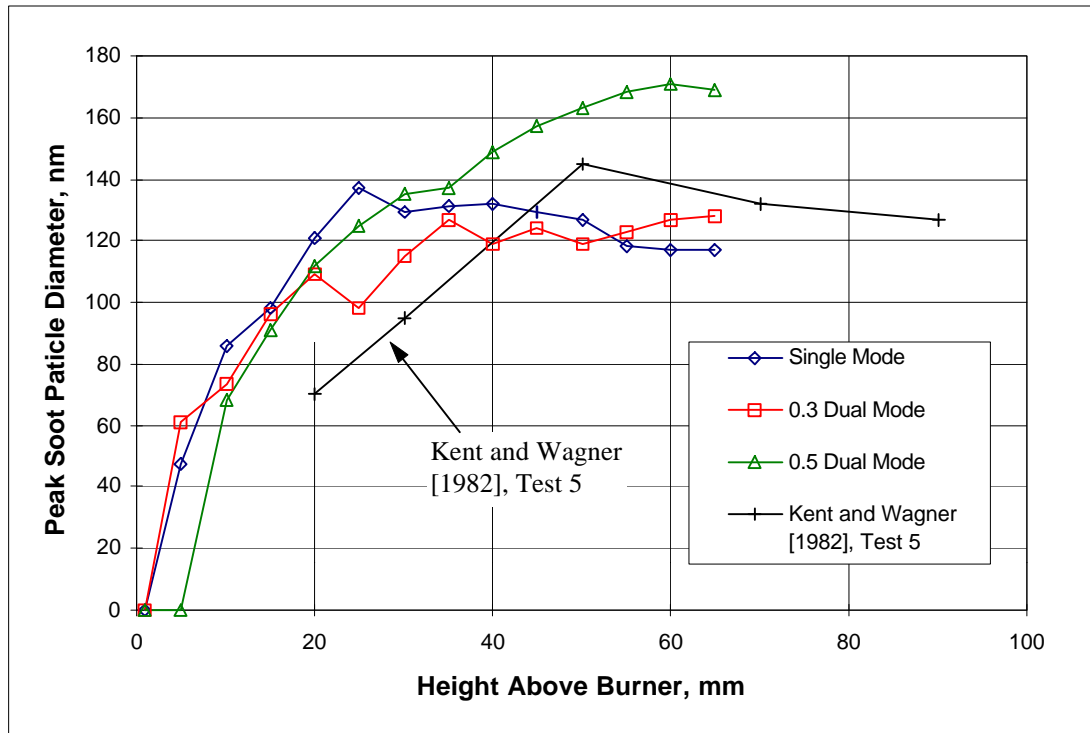


Figure 5.18 LLS Peak Soot Particle Diameters (D_{63}) vs. Height

5.3.3 Laser Light Scattering (LLS) Soot Particle Number Density

Flood plots of soot particle number density are shown in Figure 5.19, transverse profiles of soot particle number density at several heights in Figure 5.20 and peak values plotted versus height in Figure 5.21. Soot particle number densities in the single mode flame show a steady, nearly linear, increase with height in the flame where the dual mode cases peak early, near 20mm, and then slowly decline with height. Similar to the soot particle diameter analysis, these reported soot particle number densities are subject to the applicability of the Rayleigh scattering limit assumption.

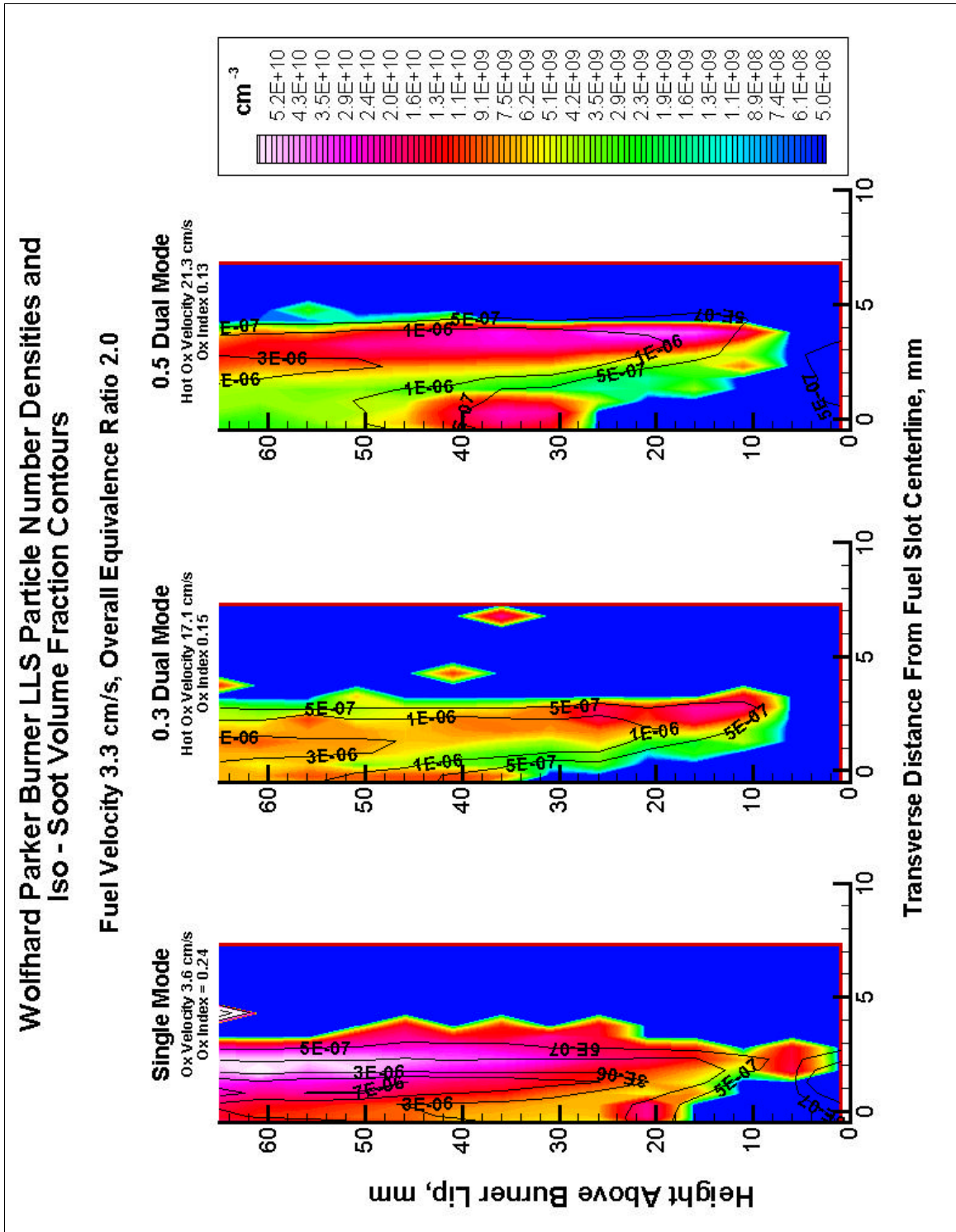


Figure 5.19 Laser Light Scattering Soot Particle Number Densities

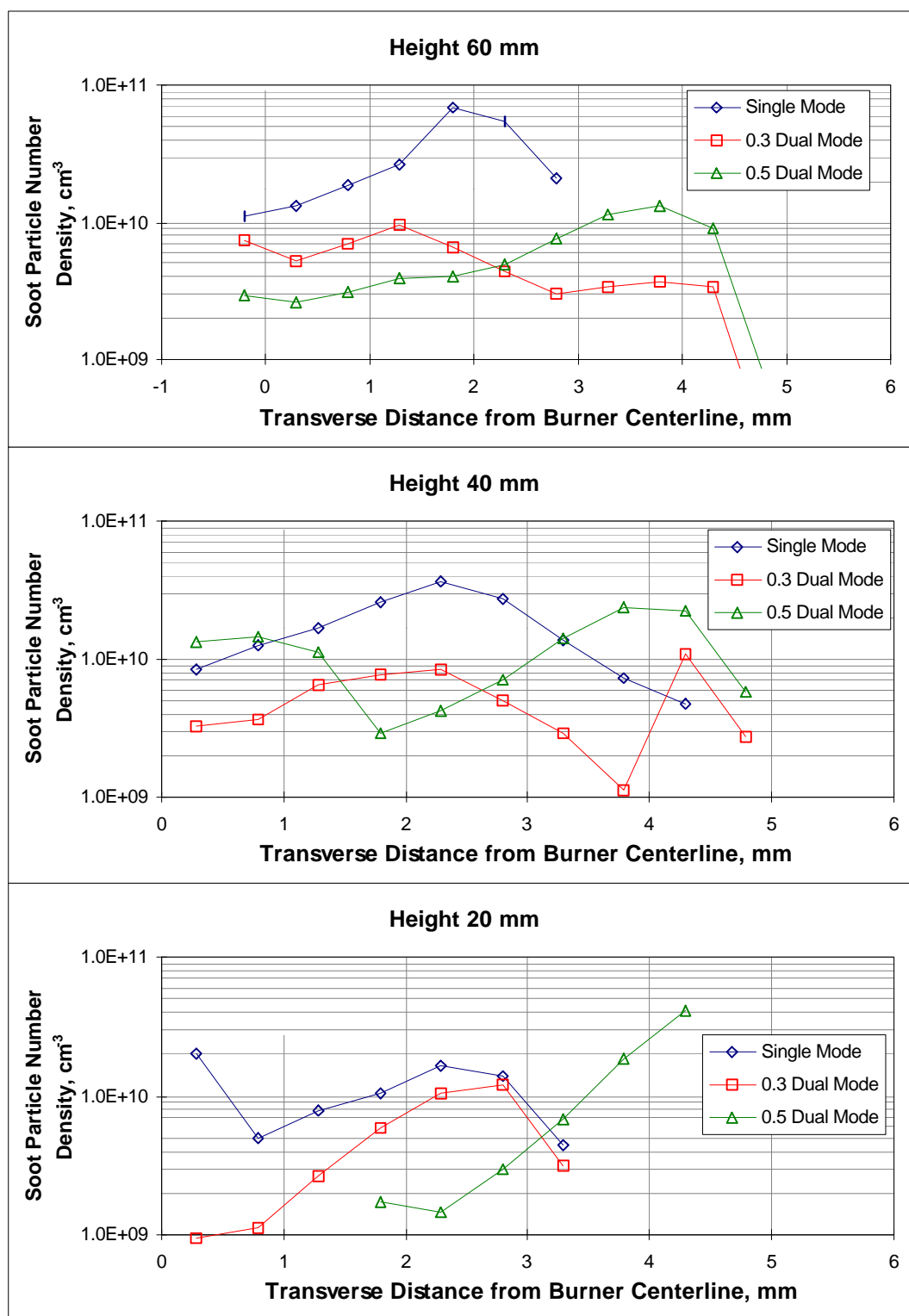


Figure 5.20 LLS Soot Particle Number Density at Various Heights

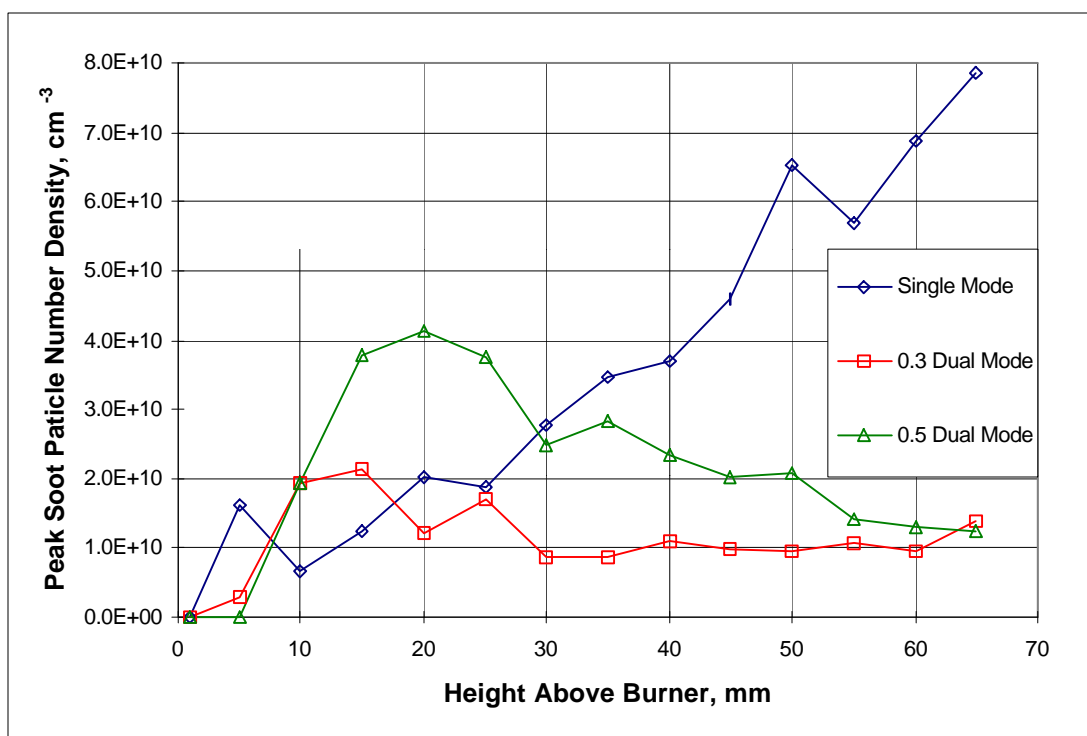


Figure 5.21 LLS Soot Particle Number Densities vs. Height

Kent and Wagner [1982] report maximum particle number densities of 2×10^{11} particles / cm^3 for their Test 5 flame; 2.5 times the maximum particle number density measured in this study's Single Mode flame, 8×10^{10} particles / cm^3 . Among the differences in scattering and extinction analysis, Lorentz-Mie versus Rayleigh, and possible differences in the flames it is difficult to quantitatively assign explanations for the differences in maximum soot particle number density between Kent and Wagner [1982] and the present study. Considering the logarithmic scales required to describe soot particle number densities in flames a factor of 2.5 is not a drastic difference.

5.4 Velocity Measurements and Calculations

As mentioned previously in Section 3.6, measurement of the complete velocity fields for the three flames was not possible because of flow seeding obstacles. The domain of seeded flow consisted of a narrow strip on the hydrocarbon fuel slot ~2 mm wide and the nitrogen coflow as shown in Figure 5.22. Width of the unseeded oxidizer regions as measured from PIV images are shown in Figure 5.23.

It is interesting to compare the coflow seeded portions of the dual mode flames to their corresponding temperature fields in Figure 5.1. The strong buoyant acceleration of the combustion gasses entrains the co-flow but it is expected that the thermophoretic potential of the flame front prevented seed particles from crossing the reaction zone.

Velocity calculations presented are only intended as rough approximations of the axial component based on the streamtube conservation of mass approach described in Section 3.6.2. Comparison of the fuel slot centerline PIV measurements with the calculated centerline velocities are shown in Figure 5.24. Agreement between measured and calculated centerline velocities is reassuring but does not guarantee accuracy of the velocity model across the full calculation domain. Centerline velocity data from the Kent and Wagner [1982] test 5 flame have been added to the Single Mode flame centerline velocity profile in Figure 5.24 showing excellent agreement between the two sets of measurements. Flood plots of calculated vertical velocities over the full calculation domain are shown in Figure 5.25. They show that although all cases had similar peak centerline velocities, ~150 cm/sec, the dual mode 0.3 case appears to have the highest overall velocities followed by the 0.5 dual mode and the single mode cases.

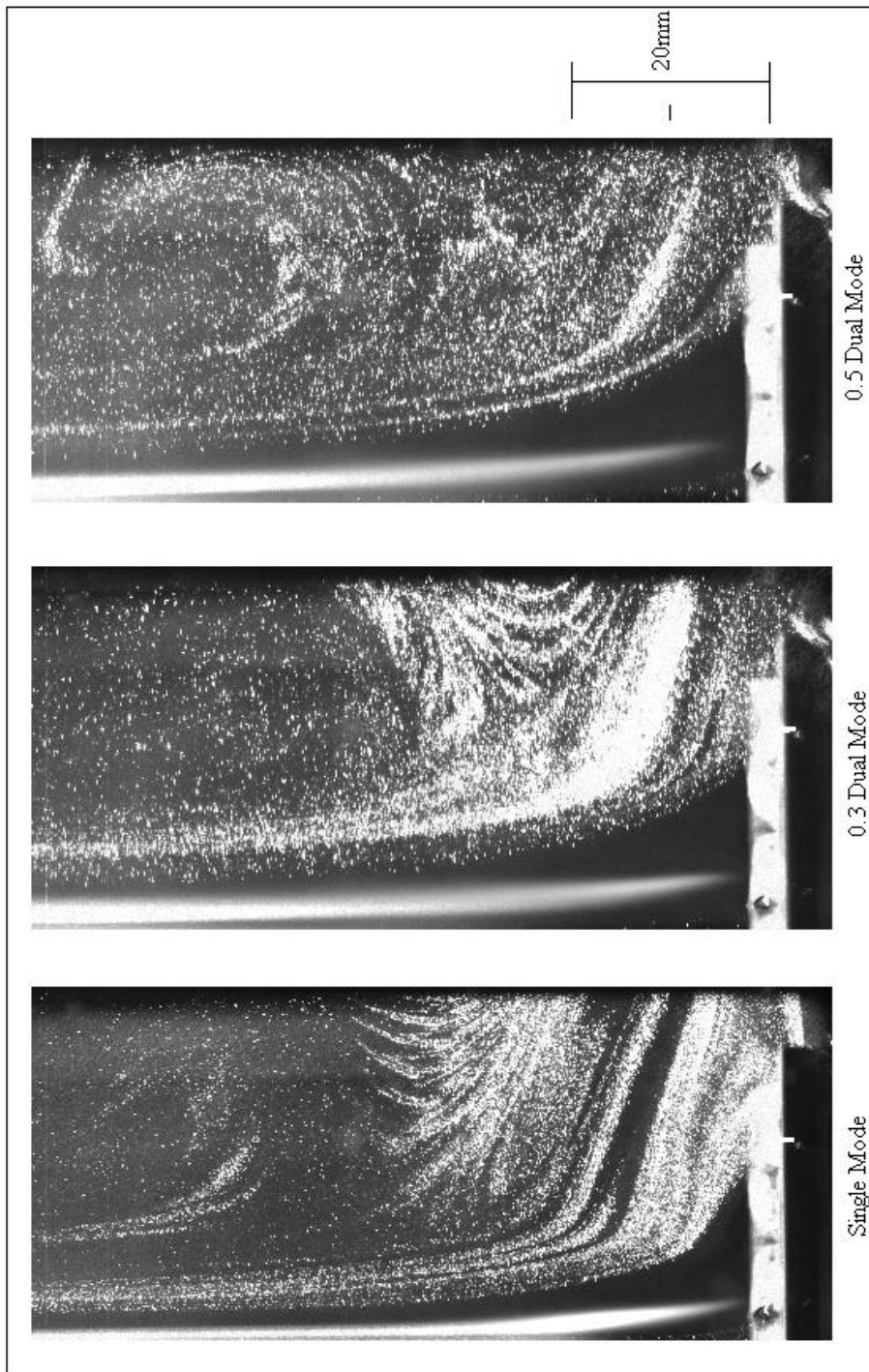


Figure 5.22 Domain of Seeded Flow for PIV Measurements (hydrocarbon fuel slot centerline on the left of each image).

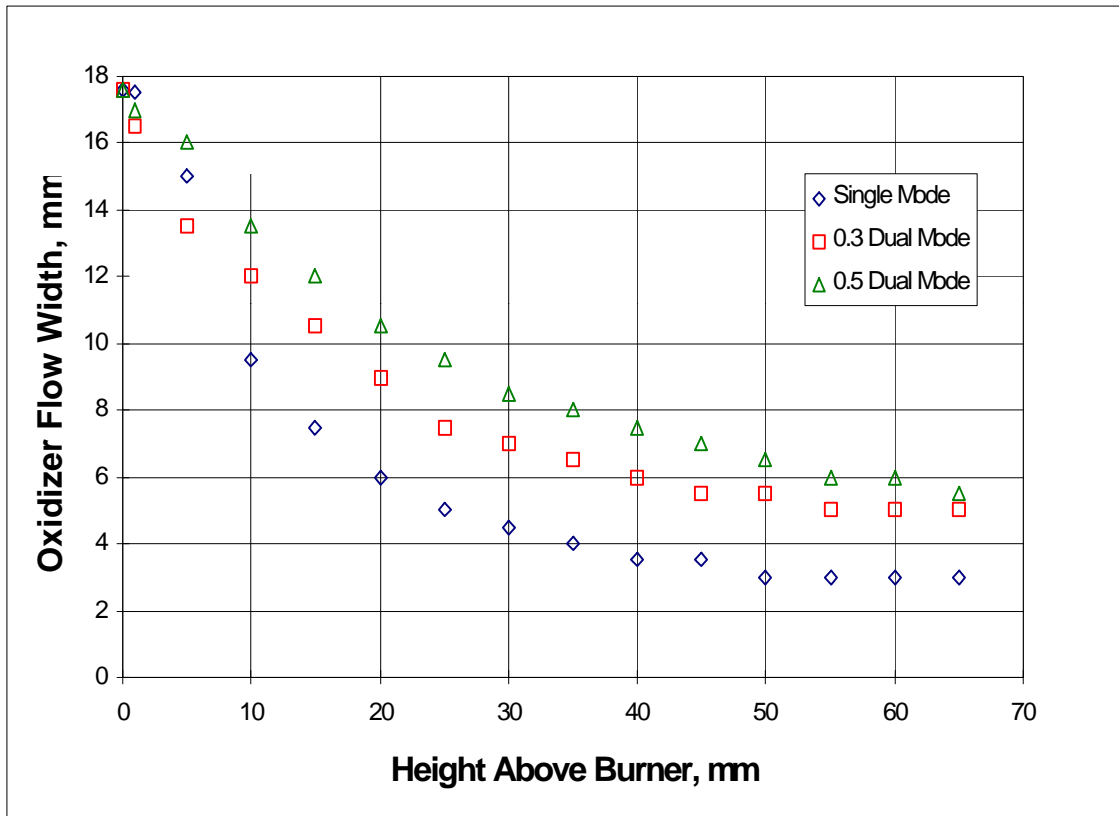


Figure 5.23 Unseeded Oxidizer Region Width for Velocity Calculations

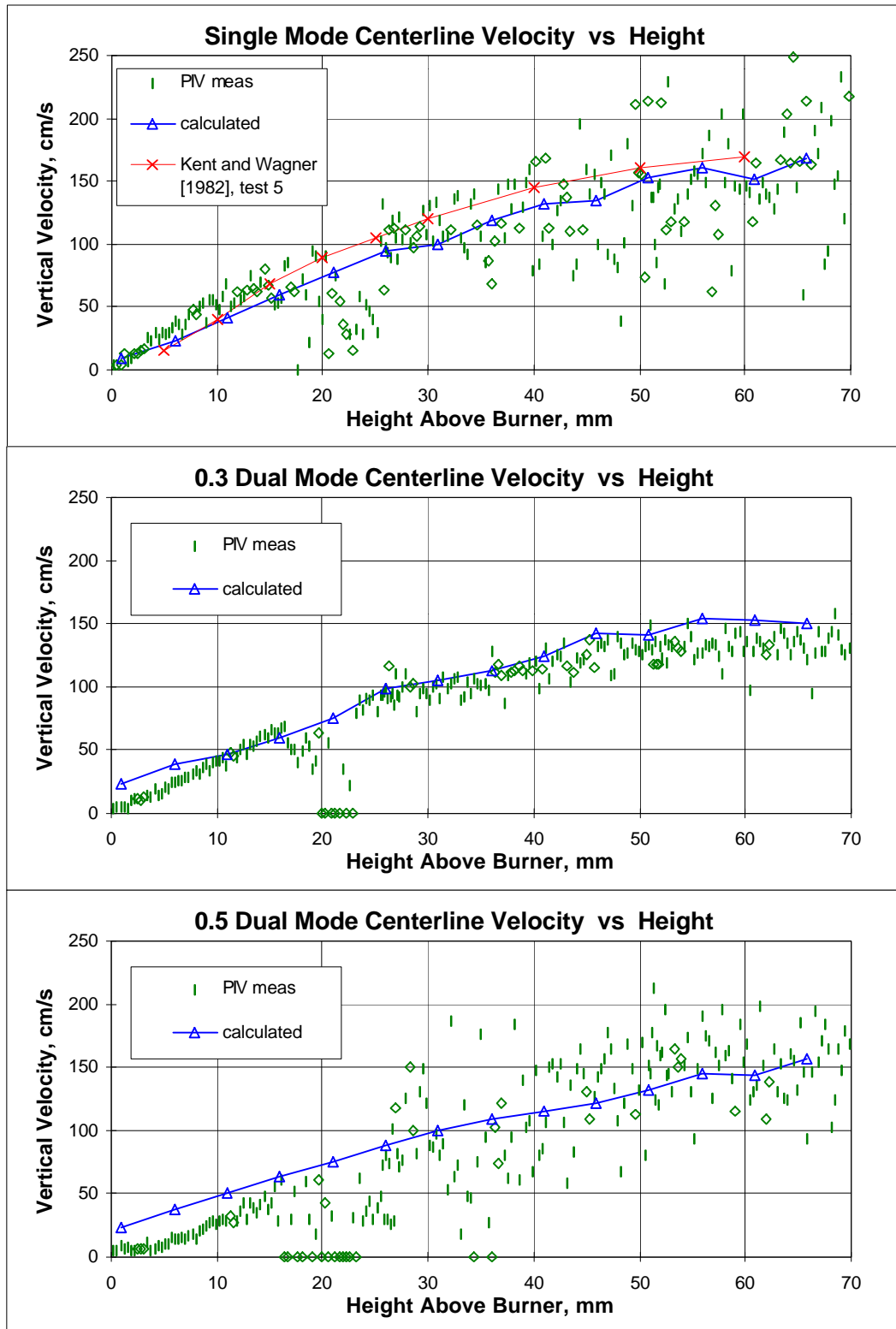


Figure 5.24 Measured and Calculated Centerline Vertical Velocities

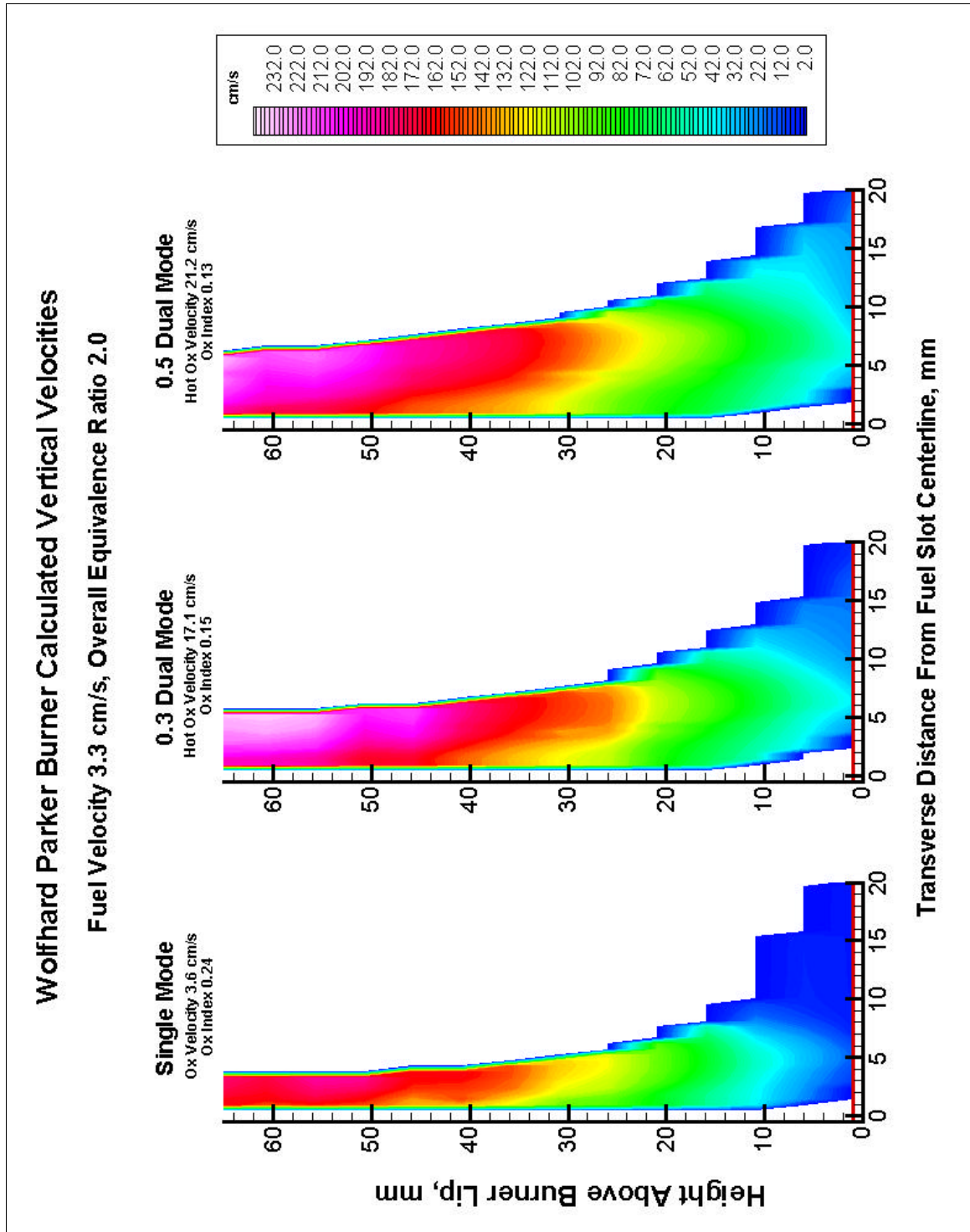


Figure 5.25 Calculated Vertical Velocities

5.5 Flux Calculations

Intensive soot concentration measurements do not necessarily indicate which flames produced the most soot on an extensive basis. To quantitatively compare overall soot loadings the soot flux must be considered. Integrated soot volume fraction (ϕ) flux, Ψ_ϕ , calculated as

$$\Psi_\phi = \int_{\text{cflow}}^{\text{centerline}} \phi (\bar{v} \cdot \hat{n}_y) dx \quad \text{Equation 5.1}$$

using the coordinates defined in Figure 3.15 is plotted as a function of height in figure 5.26. Beginning at a height of approximately 15 mm the single mode soot volume fraction flux clearly dwarfs both of the dual mode soot volume fraction flux profiles by almost a factor of two. With similar soot volume fraction and velocity distributions in the dual mode cases the extra soot laden region width of the 0.5 dual mode case appears to cause its soot volume fraction flux to be slightly higher than the 0.3 dual mode case.

Figure 5.24 shows that soot particle number density flux in the higher regions of the flame, $h > 40$ mm, was much higher for the single mode case than either of the dual mode cases. Both soot volume fraction and soot particle number density fluxes followed the same trends as the local intensive properties on which they were based. The differences in structure among the flames studied did not have large effects on their net convective transport.

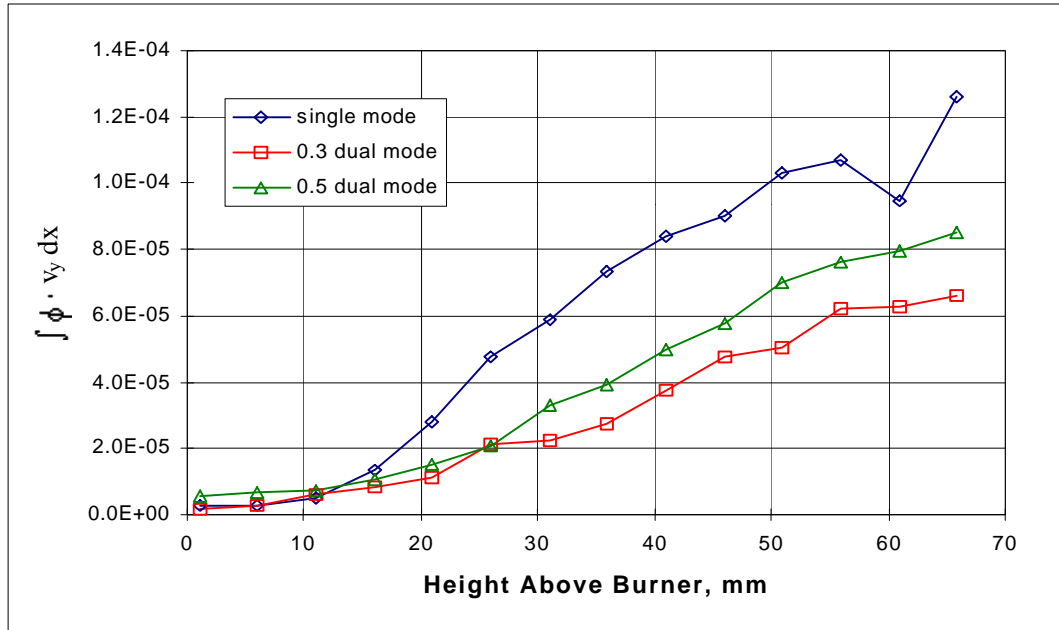


Figure 5.26 Integrated Soot Volume Fraction Flux $\{\text{cm}^2\text{s}^{-1}\}$

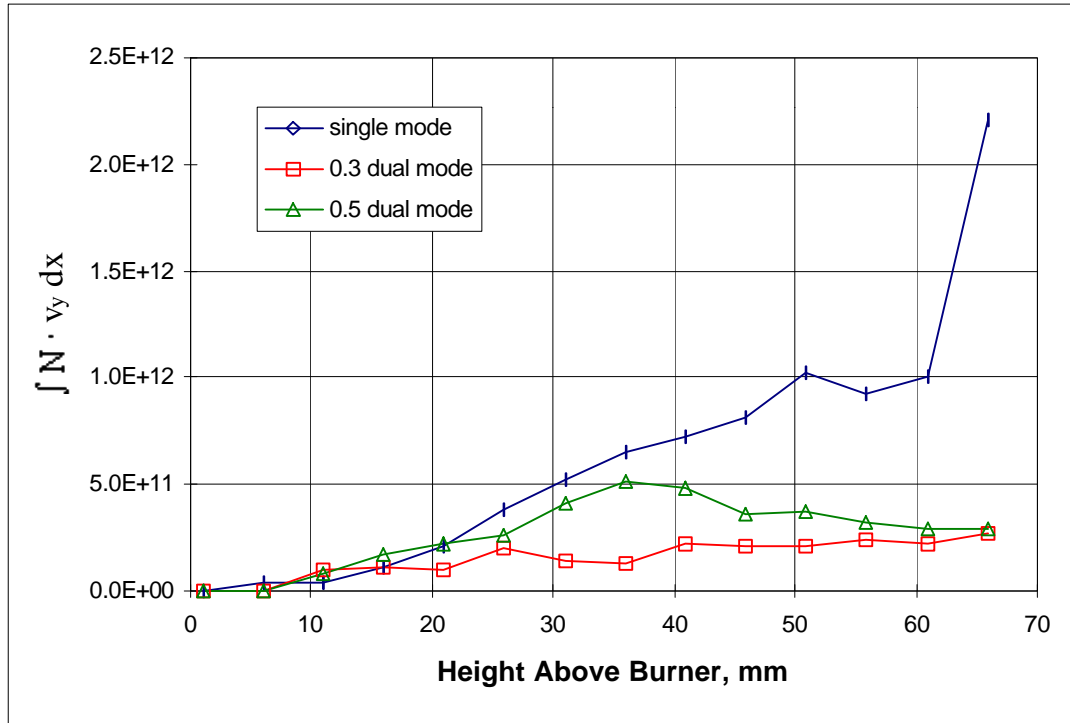


Figure 5.27 Integrated Soot Particle Number Density Flux $\{\text{particles cm}^{-1} \text{s}^{-1}\}$

5.6 Interpretation

Experience gained from the large database of single mode nonpremixed flame experiments indicate that soot loading is strongly accelerated by raising the flame temperature. This intuition fails when one tries to rationalize why dual mode flames produced drastically less soot than a single mode flame when the dual mode fuel temperatures leaving the burner was several hundred Kelvin hotter than in the single mode case and when the flame front temperatures of the dual mode cases were uniformly hotter than in the single mode case except at the point of overall maximum temperature where they matched. Clearly thermal arguments are not sufficient for explaining the observed sooting characteristics of dual mode flames.

Studies of soot oxidation have shown that the hydroxyl radical is an aggressive oxidizer of soot and soot precursors [Haudiquert, 1997, Fennimore and Jones, 1967] and even more so than either molecular or atomic oxygen [Millikan, 1962]. It is reasonable to argue that the elevated mole fractions of water vapor in the oxidizers of the dual mode cases (Table 5.1) would produce more hydroxyl at the flame front through the global reaction, $\text{H}_2\text{O} \rightarrow \text{OH} + \text{H}$, thus impeding soot formation.

Attempting to use an equilibrium analysis (STANJAN) to predict the hydroxyl concentrations at the assumed stoichiometric flame front for various heights of each case yields the results in Figure 5.28. Equilibrium analysis predicts similar hydroxyl mole fractions for the single mode and 0.3 dual mode cases with higher concentrations for the 0.5 dual mode case. The similarity between the single mode and 0.3 dual mode

equilibrium hydroxyl concentrations conflicts with the supposition that hydroxyl concentrations are the defining difference between the vastly different sooting characteristics of these two flames.

Table 5.1 Oxidizer Mole Fraction Composition

Species	Single Mode	0.3 Dual Mode, Post Premixed Flame	0.5 Dual Mode, Post Premixed Flame
H ₂ O	0.00	0.13	0.26
O ₂	0.24	0.15	0.13
N ₂	0.76	0.72	0.61

Kaskan [1958] showed by experiment that equilibrium drastically underestimates true hydroxyl concentrations and Fennimore and Jones [1967] add that the ratio of actual hydroxyl to equilibrium hydroxyl increases rapidly for decreasing values of molecular oxygen mole fraction as seen with increasing degrees of dual mode. Based on these arguments one can qualitatively infer that hydroxyl radical mole fractions increase with increasing degrees of dual mode operation yielding a plausible explanation for the fundamental sooting characteristics of single and dual mode flames.

Observations of the drastically higher particle number densities (Figure 5.19) and integrated particle number fluxes (Figure 5.27) of the highly sooting single mode flame are consistent with the past observations that soot particle inception is the overall rate limiting step [Glassman, 1988] and that “surface growth is a highly nonlinear amplifier of the original soot mass” [Dasch, 1985]. The idea of particle inception limited soot loading also corroborates the hypothesis that elevated hydroxyl concentrations at the flame front of

dual mode flames, oxidizing the earliest soot particles, could have a profound effect on the overall soot loading of the dual mode flames. For the fewer particles that evolve from the particle inception stage in dual mode flames it is reasonable to attribute their larger diameters later in the flame to reduced competition for surface growth species abundant in these underventilated flames.

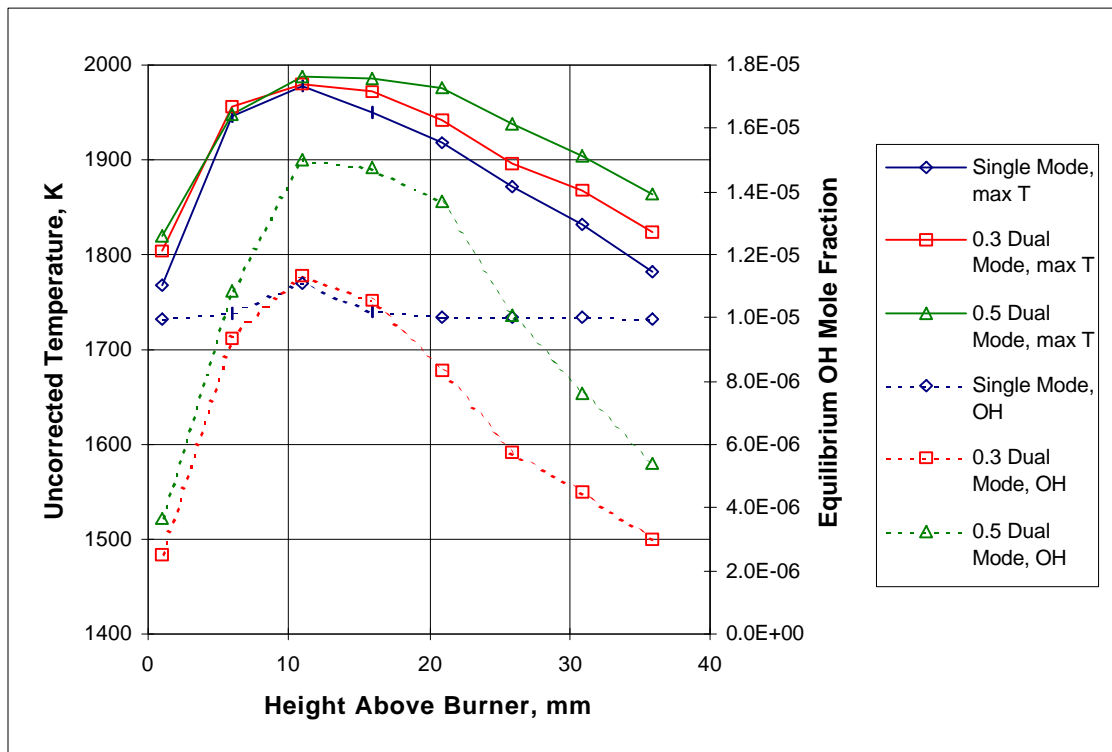


Figure 5.28 Flame Front Temperatures and Equilibrium Hydroxyl Concentrations

6.0 Conclusions and Recommendations

6.1 Summary and Conclusions

Temperature, soot and velocity measurements were performed in steady laminar nonpremixed sooting ethylene flames stabilized on a Wolfhard-Parker coflowing slot burner. The burner could be operated in single mode where a cold air/oxygen mixture was used as the oxidizer for the nonpremixed flame or in dual mode where the products of lean premixed hydrogen/air/oxygen flames were used as the oxidizer for the nonpremixed flame. Burner geometry, peak flame temperatures, nonpremixed flame fuel flow and overall burner equivalence ratio were held constant for all tests.

Dual mode operation had a marked effect on the nonpremixed flame structure broadening the flames in the transverse direction and elongating them in the axial direction. It is suspected that the broadening observed in dual mode operation is caused by shallower temperature gradients on the oxidizer side of the flame front which act to reduce transverse heat and mass diffusion velocities. Lower mass transfer rates combined with lower oxidizer oxygen indices in dual mode flames force the nonpremixed flame fuel

to diffuse greater distances to meet the oxidizer at the flame front in stoichiometric proportions.

Soot volume fractions decreased with increasing degree of dual mode operation. Peak single mode soot volume fractions were two to three times those observed in the dual mode cases and integrated soot fluxes in the single mode flame was nearly twice that of the dual mode flames. Soot particle number densities decreased from single to dual mode operation with the 0.3 dual mode case having slightly lower peak soot particle number densities and lower integrated soot particle fluxes than 0.5 dual mode flame. The 0.5 dual mode case yielded the largest soot particle diameters with single mode and 0.3 dual mode flames producing similarly smaller peak soot particle diameters.

Lower soot loadings observed in the dual mode cases are presumed to be the result of aggressive oxidation of young soot particles and soot growth species by elevated hydroxyl concentrations on the fuel side of the flame front. Recalling that particle inception is accepted as the overall soot formation rate limiting process, it makes sense that the fewer particles escaping a hydroxyl rich region near the flame front in dual mode operation would yield overall lower soot loadings. The larger soot particle diameters observed in the dual mode cases are attributed to less competition for surface growth species because of their lower particle number densities compared to single mode flames.

Thermocouple Particle Densitometry soot volume fraction measurements produced results remarkably similar to laser light extinction measurements which were regarded as the standard. Implementation of TPD with existing rapid insertion temperature measurement algorithms was very simple and a worth while endeavor.

Particle imaging velocimetry was less than ideal for making velocity measurements in the flames studied. The sparse seeding and strong accelerations observed in the flames may have better suited the Laser Doppler Velocimetry technique.

Accurate values of thermocouple junction Nusselt numbers are critical in making meaningful gas temperature calculations based on thermocouple thermometry in low Reynolds number ($Re_d < 1.0$) combustion environments. A novel method of estimating thermocouple junction Nusselt numbers relative to a standard spherical junction was developed and implemented but not formally verified (Appendix A).

6.2 Recommendations for Future Work

- Soot particle diameters observed in this study were well in excess of those deemed acceptable for Rayleigh scattering analysis. Implementation of the full Lorentz-Mie theory for interaction of light with spheres would improve the quantitative accuracy of the optical soot characterization. Tunneling Electron Microscopy imaging of soot agglomerates sampled from the flame would complement the laser light scattering and extinction measurements and chemical species measurements (particularly the hydroxyl radical) would have aided interpretation of the results.
- The sooting characteristics observed in this study were the result of both thermal and chemical effects. Measurements in similar nonpremixed flames with heated but *non-vitiated* oxidizers of comparable temperatures to the present study would allow the thermal effect to be isolated and studied. Design of a non-vitiating air heater that can achieve steady output temperatures greater than 1000 K is a formidable challenge.

- Hydrogen was chosen as the premixed flame fuel for this study because of its chemical simplicity. The only new chemical species added by the premixed flame products in appreciable quantities was water vapor. Using hydrocarbons as premixed flame fuels would add both water vapor and carbon dioxide to the oxidizer stream better simulating the effect of fuel rich regions burning in the wake of previously burned hydrocarbon/air mixtures. Considering an array of hydrocarbon fuels may also reveal interesting differences in the soot formation chemistry.
- Any continuation of this work should proceed in parallel with a modeling effort, especially considering that one of the major goals of this project was to provide model validation data. Computation of chemical species that cannot be practically measured would greatly assist in the interpretation and understanding of the soot chemistry in these flames.
- The burner in this study was designed to fit into a high pressure vessel owned by the Reacting Flows Laboratory at Virginia Tech. High pressure operation would further improve burner's ability to simulate combustion processes in practical combustion devices.

References

- Acrivos, A. and T. D. Taylor, "Heat and Mass Transfer from Single Spheres in Stokes Flow," *The Physics of Fluids*, Volume 5, Number 4, 387 (1962).
- Aftel, R., "Soot Formation in Single and Dual-Mode Counterflow Flames," Doctoral Dissertation, Virginia Polytechnic Institute and State University, Blacksburg, Virginia (1996).
- Barr, J. and B. P. Mullins, "Combustion in vitiated atmospheres I - Combustion process in vitiated air," *Fuel*, Volume XXVIII, Number 8, 181 (1950).
- Barr, J., "Combustion in vitiated atmospheres II - Some preliminary studies of diffusion flames," *Fuel*, Volume XXVIII, Number 9, 200 (1950).
- Barr, J. and B. P. Mullins, "Combustion in vitiated atmospheres IV - Performance of a typical combustion chamber," *Fuel*, Volume XXVIII, Number 10, 225 (1950).
- Barr, J. and B. P. Mullins, "Combustion in vitiated atmospheres V - Application of results," *Fuel*, Volume XXVIII, Number 10, 228 (1950).
- Bohren, C. F. and D. R. Huffman, Absorption and Scattering of Light by Small Particles, New York: Wiley (1983).
- Bradley, D. and A. G. Entwistle, "Determination of the Emissivity, for Total Radiation, of Small Diameter Platinum - 10% Rhodium Wires in the Temperature Range 600 - 1450 °C," *British Journal of Applied Physics*, Volume 12, 708 (1961).
- Bradley, D. and A. G. Entwistle, "The Total Hemispherical Emittance of Coated Wires," *British Journal of Applied Physics*, Volume 17, 1155 (1966).

- Bradley, D. and K. J. Matthews, "Measurement of High Gas Temperatures with Fine Wire Thermocouples," *Journal of Mechanical Engineering Science*, Volume 4, 229 (1968).
- Burke, S. P. and T. E. W. Schumann, "Diffusion Flames," *Industrial & Engineering Chemistry*, Volume 20, 998 (1928).
- Calcote, H. F., "Mechanisms of Soot Nucleation in Flames - A Critical Review," *Combustion and Flame*, Volume 42, 215 (1981).
- Choi, M. Y., G. W. Mulholland, A. Hamins and T. Kashiwagi, "Comparisons of the Soot Volume Fraction Using Gravimetric and Light Extinction Techniques," *Combustion and Flame*, Volume 102, 161 (1995).
- Collis, D. C., and M. J. Williams, "Two-dimensional Convection from Heated Wires at Low Reynolds Numbers," *Journal of Fluid Mechanics*, Volume 6, 357 (1959).
- Dalzell, W. H. and A. F. Sarofim, *Transactions of the ASME, Journal of Heat Transfer*, Volume 91, 100 (1969).
- Dasch, C. J., "The Decay of Soot Surface Growth Reactivity and Its Importance in Total Soot Formation," *Combustion and Flame*, Volume 61, 219 (1985).
- Eisner, A. D. and D. E. Rosner, "Experimental Studies of Soot Particle Thermophoresis in Nonisothermal Combustion Gases Using Thermocouple Response Techniques," *Combustion and Flame*, Volume 61, 153 (1985).
- Fenimore, C. P. and G. W. Jones, "Oxidation of Soot by Hydroxyl Radicals," *The Journal of Physical Chemistry*, Volume 71, Number 3, 593 (1967).
- Flower, W. L., "The Effect of Elevated Pressure on the Rate of Soot Production in Laminar Diffusion Flames," *Combustion Science and Technology*, Volume 48, 31 (1986).
- Flower, W. L., "An Investigation of Soot Formation in Axisymmetric Turbulent Diffusion Flames at Elevated Pressure," *Twenty-Second Symposium (International) on Combustion*, The Combustion Institute, 425 (1988).
- Frenklach, M., "On Surface Growth Mechanisms of Soot Particles," *Twenty-Sixth Symposium (International) on Combustion*, The Combustion Institute, 1996.

- Glassman, I. and P. Yaccarino, "The Temperature Effect in Sooting Diffusion Flames," *Eighteenth Symposium (International) on Combustion*, The Combustion Institute, 1175 (1981).
- Glassman, I., "Soot Formation in Combustion Processes," *Twenty-Second Symposium (International) on Combustion*, The Combustion Institute, 295 (1988).
- Govatzidakis, G. J., "Thermocouple Thermometry in Soot Bearing Flames," Bachelor of Science Thesis, Mechanical Engineering Department, Brown University (1993).
- Harris, S. J., A. M. Weiner and C. C. Ashcraft, "Soot Particle Inception Kinetics in a Premixed Ethylene Flame," *Combustion and Flame*, Volume 64, 65 (1986).
- Haudiquert, M., A. Cessou, D. Stepowski and A. Coppalle, "OH and Soot Concentration Measurements in a High-Temperature Laminar Diffusion Flame," *Combustion and Flame*, Volume 111, 338 (1997).
- Haynes, B. S. and Wagner H. Gg., "Sooting Structure in a Laminar Diffusion Flame," *Ber. Bunsenges. Phys. Chem.*, Volume 84, 499 (1980).
- Haynes, B. S. and Wagner H. Gg., "Soot Formation," *Progress in Energy and Combustion Science*, Volume 7, 229 (1981).
- Hura, H. S. and I. Glassman, "Soot Formation in Diffusion Flames of Fuel/Oxygen Mixtures," *Twenty-Second Symposium (International) on Combustion*, The Combustion Institute, 371 (1988).
- Kang, K. T., J. Y. Hwang, S. H. Chung and W. Lee, "Soot Zone Structure and Sooting Limit in Diffusion Flames: Comparison of Counterflow and Co-flow Flames," *Combustion and Flame*, Volume 109, 266 (1997).
- Kaskan, W. E., "The Dependence of Flame Temperature on Mass Burning Velocity," *Sixth Symposium (International) on Combustion*, The Combustion Institute, 134 (1957).
- Kaskan, W. E., "Hydroxyl Concentrations in Rich Hydrogen-Air Flames Held on Porous Burners," *Combustion and Flame*, Volume 2, 229 (1958).
- Kent, J. H., H. Jander and H. Gg. Wagner, "Soot Formation in a Laminar Diffusion Flame," *Eighteenth Symposium (International) on Combustion*, The Combustion Institute, 1117 (1981).

- Kent, J. H. and H. Gg. Wagner, "Soot Measurements in Laminar Ethylene Diffusion Flames," *Combustion and Flame*, Volume 47, 53 (1982).
- Kent, J. H. and H. Gg. Wagner, "Why Do Diffusion Flames Emit Smoke?," *Combustion Science and Technology*, Volume 41, 245 (1984a).
- Kent, J. H. and H. Gg. Wagner, "Temperature and Fuel Effects in Sooting Diffusion Flames," *Twentieth Symposium (International) on Combustion*, The Combustion Institute, 1007 (1984b).
- Kerker, M., The Scattering of Light and Other Electromagnetic Radiation, New York: Academic Press (1969).
- Lahaye, J. and G. Prado, "Mechanisms of Carbon Black Formation," in Walker, P. L. and P. A. Throver (Eds.), Chemistry and Physics of Carbon, New York: Marcell Dekker, Volume 14, pp168 - 294.
- Lahaye, J. and G. Prado, Soot in Combustion Systems and its Toxic Properties, New York: Plenum Press (1983).
- Madson, J. M. and E. A. Theby, "SiO₂ Coated Thermocouples," *Combustion Science and Technology*, Volume 36, 205 (1984).
- McEnally, C. S., Ü. Ö. Köylü, L. D. Pfefferle and D. E. Rosner, "Soot Volume Fraction and Temperature Measurements in Laminar Nonpremixed Flames Using Thermocouples," *Combustion and Flame*, Volume 109, 701 (1997).
- Millikan, R. C., "Non-Equilibrium Soot Formation in Premixed Flames," *The Journal of Physical Chemistry*, Volume 66, 794 (1962).
- Moss, J. B., C. D. Stewart and K. J. Syed, "Flowfield Modelling of Soot Formation at Elevated Pressure," *Twenty-Second Symposium (International) on Combustion*, The Combustion Institute, 413 (1988).
- Moss, J. B., C. D. Stewart and K. J. Young, "Modeling Soot Formation and Burnout in a High Temperature Laminar Diffusion Flame Burning under Oxygen-Enriched Conditions," *Combustion and Flame*, Volume 101, 491 (1995).
- Mullins, B. P., "Combustion in vitiated atmospheres III - Effect of oxygen concentration on ignition induction period," *Fuel*, Volume XXVIII, Number 9, 205 (1950).

- Norton, T. S., K. C. Smyth, J. H. Miller and M. D. Smooke, "Comparison of Experimental and Computed Species Concentration and Temperature Profiles in Laminar, Two-Dimensional Methane/Air Diffusion Flames," *Combustion Science and Technology*, Volume 90, 1 (1993).
- Peters, N., "Laminar Flamelet Concepts in Turbulent Combustion," *Twenty-first Symposium (International) on Combustion*, The Combustion Institute, 1231 (1986).
- Rao, V. K and M. F. Bardon, "The Effect of Water on Gas Phase Soot Formation in Laminar Diffusion Flames," *Combustion and Flame*, Volume 55, 73 (1984).
- Rosner, D. E., Transport Processes in Chemically Reacting Flow. Boston: Butterworth Publishers (1986).
- Smith, O. I., "Fundamentals of Soot Formation in Flames with Application to Diesel Engine Particulate Emissions," *Progress in Energy and Combustion Science*, Volume 7, 275 (1981).
- Smyth, K. C., J. H. Miller, R. C. Dorfman, W. G. Mallard and R. J. Santoro, "Soot Inception in a Methane / Air Diffusion Flame as Characterized by Detailed Species Profiles," *Combustion and Flame*, Volume 62, 157 (1985).
- Smyth, K. C., P. J. H. Tjossem, A. Hamins and J. H. Miller, "Concentration Measurements of OH· and Equilibrium Analysis in a Laminar Methane - Air Diffusion Flame," *Combustion and Flame*, Volume 79, 366 (1990).
- Smyth, K. C. and C. R. Shaddix, "The Elusive History of $\tilde{n} = 1.57 - 0.56i$ for the Refractive Index of Soot," *Combustion and Flame*, Volume 107, 314 (1996).
- Santoro, R. J., H. G. Semerjian and R. A. Dobbins, "Soot Particle Measurements in Diffusion Flames," *Combustion and Flame*, Volume 51, 203 (1983).
- Talley, D. G., "Some Properties of Nearly Premixed Laminar Flame Propagation Along Weakly Stratified Layers in Combustible Gas Mixtures," *Combustion and Flame*, Volume 79, 141 (1990).
- Tien, C. L. and S. C. Lee, "Flame Radiation," *Prog. Energy Combust. Sci.*, Volume 8, 41 (1982).
- Vander Wal, R. L., "A TEM Methodology for the Study of Soot Particle Structure," *Combustion Science and Technology*, Volume 126, 333 (1997).

- Vandsburger, U., I. Kennedy and I. Glassman, "Sooting Counterflow Diffusion Flames with Varying Oxygen Index," *Combustion Science and Technology*, 39, 263 (1984).
- Vandsburger, U., "An Experimental Study of the Processes Involved in the Formation of Soot Particles in Diffusion Flames," Doctoral dissertation, Princeton University, Princeton, New Jersey (1986).
- Vliet, G. C. and G. Leppert, "Forced Convection Heat Transfer From an Isothermal Sphere to Water," *Journal of Heat Transfer, Transactions of the American Society of Mechanical Engineers, Series C*, Volume 83, 163 (1961).
- Wagner, H. Gg., "Soot Formation in Combustion," *Seventeenth Symposium (International) on Combustion*, The Combustion Institute, 3 (1979).
- Wagner, H. Gg., "The Influence of Pressure on Soot Formation," *AGARD Conference Proceedings*, Number 422, 24-1 (1987).
- Wey, C., E. A. Powell and J. I. Jagoda, "The Effect on Soot Formation of Oxygen in the Fuel of a Diffusion Flame," *Twentieth Symposium (International) on Combustion*, The Combustion Institute, 1017 (1984a).
- Wey, C., A. Powell and J. I. Jagoda, "The Effect of Temperature on the Sooting Behavior of Laminar Diffusion Flames," *Combustion Science and Technology*, Volume 41, 173 (1984b).
- Whitaker, S., "Forced Convection Heat Transfer Correlations for Flow in Pipes, Past Flat Plates, Single Clinders, Single Spheres, and for Flow in Packed Beds and Tube Bundles," *AIChE Journal*, Volume 18, Number 2, 361 (1972).
- Wolfhard, H. G. and W. G. Parker, "A Spectroscopic Investigation into the Structure of Diffusion Flames," *Proc. Phys. Soc.*, A65, 2 (1952).
- Wright, C. P., Applied Measurement Engineering: How to Design Effective Mechanical Measurement Systems, Englewoods Cliffs, NJ: Prentice Hall (1995).
- Zhang, C., A. Atreya and K. Lee, "Sooting Structure of Methane Counterflow Diffusion Flames with Preheated Reactants and Dilution by Products of Combustion," *Twenty-Fourth Symposium (International) on Combustion*, The Combustion Institute, 1049 (1992).